ResearchGate

See discussions, stats, and author profiles for this publication at: https://www.researchgate.net/publication/44887153

Non-Born-Oppenheimer quantum chemistry on the fly with continuous path branching due to nonadiabatic and intense optical interactions. J. Chem. Phys. 132, 244102

ARTICLE *in* THE JOURNAL OF CHEMICAL PHYSICS · JUNE 2010

Impact Factor: 2.95 · DOI: 10.1063/1.3439396 · Source: PubMed

CITATIONS
17

READS
57

2 AUTHORS, INCLUDING:

Kazuo Takatsuka
The University of Tokyo
160 PUBLICATIONS **2,676** CITATIONS

SEE PROFILE

Available from: Kazuo Takatsuka
Retrieved on: 16 January 2016

Non-Born–Oppenheimer quantum chemistry on the fly with continuous path branching due to nonadiabatic and intense optical interactions

Takehiro Yonehara[a] and Kazuo Takatsuka[b]
Department of Basic Science, The University of Tokyo, Komaba, 153-8902 Tokyo, Japan

(Received 26 January 2010; accepted 10 May 2010; published online 22 June 2010)

We extend our formerly proposed theory for non-Born–Oppenheimer electronic and nuclear wavepacket dynamics within on-the-fly scheme [T. Yonehara, S. Takahashi, and K. Takatsuka, J. Chem. Phys. **130**, 214113 (2009)] to a case of nonadiabatic dynamics under an intense laser field: electron wavepacket in a molecule is propagated in attosecond time-scale along non-Born–Oppenheimer nuclear paths that smoothly branch due to nonadiabatic coupling and/or optical interactions. Such branching paths are determined consistently with the motion of the electron wavepackets. Furthermore, these nuclear paths are quantized in terms of Gaussian wavepackets (action decomposed function), which can be applied to nonclassical paths. Both electronic wavepacket dynamics and quantization of non-Born–Oppenheimer paths are generalized so as to include the direct effects of the classical vector potential of electromagnetic fields. In the second half of this paper, we perform numerical studies to explore nonadiabatic dynamics in a laser field by examining two cases: one is a two-state model system having an avoided crossing, and the other is two-state dynamics in HF molecule on the two low lying *ab initio* potential curves. Both are placed in laser fields. With the former system, we survey some basic properties of the coupling of nonadiabatic dynamics and laser interaction varying the relevant coupling parameters such as the laser timing with respect to the incident of nonadiabatic transition. This investigation will set a foundation for the future studies of control of electronic states in realistic multidimensional molecular systems. Application to the latter system shows that non-Born–Oppenheimer quantum chemistry in laser fields is indeed useful in the study of dynamics in *ab initio* level. Through the comparison with full quantum data, we verify that the formalism and methodology developed here work accurately. Furthermore, we attain some basic insight about the characteristics of molecules in laser fields. © *2010 American Institute of Physics*. [doi:10.1063/1.3439396]

I. INTRODUCTION

Most of the chemical dynamics on electronically excited states is triggered by pulse lasers and quite often undergo nonadiabatic transitions between many states in the course of dynamics.[1–6] The studies of such dynamics have been enhanced by the rapid progress of laser technology, which can now create an ultrashort pulse down to the order of 10 as and/or an intense field higher than 10^{16} W/cm^2. These lasers can affect chemical dynamics by significantly modulating the electronic states. For instance, a pulse of the order of 10 as is short enough to trigger and track the electron wavepacket dynamics, and the intense laser can create new electronic wavepacket states.

Since such a strong laser field can also strongly affect the nuclear motion inside a molecule, a new type of nonadiabatic (kinematic) interaction between electrons and nuclei is expected to emerge. Indeed, we have shown that an infrared laser can induce electronic excitation very efficiently through such kinematic coupling, which is usually not efficient if the coupling is neglected and/or the laser field is weak.[7] Besides, the induced nonadiabatic coupling by intense laser can further couple with the native nonadiabatic interactions that are ubiquitous in the electronically excited states. Therefore there is a strong need to develop the study of nonadiabatic electron wavepacket dynamics in laser fields, and the aim of this paper is to propose a theory of electronic and nuclear wavepacket dynamics in the so-called on-the-fly scheme in classical vector potentials.

As for nonadiabatic transition in vacuum, there have been proposed many beautiful and powerful theories (for recent reviews, see Refs. 8–13). The semiclassical theories such as the Landau–Zener classic ansatz are successfully applied mostly in one-dimensional slice of the potential functions in the direction perpendicular to the crossing manifold.[14–18] On the other hand, powerful and practical techniques such as the surface-hopping[19,20] and spawning methods[21–26] and their variants have been proposed to handle multidimensional nonadiabatic transitions. Another kind of nonadiabatic transition is based on the electronic wavepacket propagation on smooth "classical" paths. The semiclassical Ehrenfest theory (SET) is an illuminating example of this category.[27,28] Yet, to overcome the unphysical paths generated in SET, Truhlar and his co-workers proposed a theory of "natural decoherence" to generate a non-Born–Oppenheimer path that passes through a nonadiabatic region smoothly from one adiabatic potential energy surface to another.[29–31]

[a]Electronic mail: yota@mns2.c.u-tokyo.ac.jp.
[b]Electronic mail: kaztak@mns2.c.u-tokyo.ac.jp.

 © 2010 American Institute of Physics

Miller and his co-workers developed semiclassical theory for nonadiabatic transition that fits in the initial value representation.[32,33]

Recently we have proposed an idea of treating nonadiabatic transition based on the dynamics of electronic wavepacket bifurcation. In this theory, nuclear paths naturally branch simultaneously with electronic wavepacket bifurcation in the nonadiabatic region, and each of them eventually proceeds to one of the adiabatic potential energy surfaces asymptotically. These nuclear dynamics is driven by a generalized classical force in a matrix form.[34] To handle the infinitely many cascades of branching (non-Born–Oppenheimer) paths, we also have proposed an approximation that takes an average of them in phase space. This scheme is called phase-space averaging and natural branching (PSANB) method.[35] The paths thus generated are smoothly connected throughout the entire space and naturally branch eventually and thereby represent the quantum entanglement between electrons and nuclei in a mixed quantum and classical representation. The entanglement is an essential feature of nonadiabatic transition, which is originated from wavepacket bifurcation. Furthermore, these branching nonclassical paths are quantized in terms of our formerly proposed semiclassical mechanics based on action decomposed function (ADF).[36] Actually we use a Gaussian function to represent each of such wavepackets, which we call normalized variable Gaussian (NVG), since NVG can be applied to nonclassical paths such as ours generated in PSANB procedure.[37,38] In this way, we can build a total wave function composed of the pieces of electronic and nuclear wavepackets. In this function, not only the probability amplitude but a set of quantum phases are appropriately taken into account. This theoretical scheme, which we call PSANB-ADF-NVG method, has already been numerically verified and implemented into an *ab initio* level of quantum chemical package.

In this paper, we report on an extension of PSANB-ADF-NVG scheme to a case of molecular nonadiabatic interaction in classical vector potentials. We have studied before the effect of intense laser fields on polyatomic molecules within the level of SET,[7,39] from which much interesting insight about interplay between laser field and electron-nuclei kinematic coupling has been deduced. The present extension beyond the SET approximation will further prevail the novel features of the (native and induced) nonadiabatic interactions in laser fields. Therefore the present work is designed to set a theoretical foundation for our extensive applications in this field.

In the last half of this paper, we present numerical studies on the basis of the present theory. We verify the theory by comparing various quantities provided by the present scheme with their counterparts given by full quantum calculations with the use of a simple model system and HF molecule in an *ab initio* level of calculation. However, we preclude ionization process in this treatment. This aspect of the study is underway in our laboratory.

The rest of this paper is organized as follows. In Sec. II, we briefly study an extension of PSANB scheme to a system including laser fields. Section III presents the quantization of the branching paths in terms of ADF-NVG. To do so, we carefully examine and confirm that the equations of motion for ADF should hold in the same form as in the field-free case. Section IV presents numerical illustrations that feature the various aspects of interaction between nonadiabatic transition and laser coupling. This paper concludes in Sec. V.

II. ELECTRON WAVEPACKETS PROPAGATED ALONG BRANCHING NUCLEAR PATHS

We first outline our theoretical scheme. In case where no laser field is applied, the total wave function is expanded as[40]

$$\Psi(\mathbf{r},\mathbf{R},t)=\sum_I \chi_I(\mathbf{R},t)\Phi_I(\mathbf{r};R), \tag{1}$$

where the independent variables $\mathbf{r}$ and $\mathbf{R}$ stand for the electronic and nuclear coordinates, respectively, and t stand for time. The electronic bases $\Phi_I(\mathbf{r};\mathbf{R})$, either adiabatic or diabatic, are generated at each nuclear position and is time independent. The coefficient functions $\chi_I(\mathbf{R},t)$ in this expansion are supposed to represent the nuclear dynamics, which is usually treated as unknown functions (see Appendix A). The dependence of $\Phi_I(\mathbf{r};\mathbf{R})$ on $\mathbf{R}$ parametrically manifests the spirit of the fixed nuclei (Born–Oppenheimer) approximation (see Ref. 41 for a recent analysis on the reason why the Born–Oppenheimer approximation is so good.) As seen above, however, any time-dependence is rendered only to the nuclear part $\chi_I(\mathbf{R},t)$. In principle the completeness of the set $\{\Phi_I(\mathbf{r};\mathbf{R})\}$ ensures that Eq. (1) could represent any time-dependent state of a molecule. However, an explicit time-dependent representation also for the electronic state should be much more appropriate, when an ultrashort pulse laser of the attosecond time-scale is applied, since its time-scale is comparable with that of the electronic motion within a molecule.

On the basis of the above observation, we would like to propagate the nuclear and electronic wavepackets along nuclear paths, which is called on-the-fly scheme. More explicitly, the total wave function should be represented as

$$\Psi(\mathbf{r},\mathbf{R},t)=\sum_K^{\text{state}}\sum_k^{\text{path}}\Phi_K(\mathbf{r},t;\mathbf{R}_{Kk}(t))\chi_{Kk}(\mathbf{R}-\mathbf{R}_{Kk}(t),t), \tag{2}$$

where the time-dependent electronic wave function $\Phi_K(\mathbf{r},t;\mathbf{R}_{Kk}(t))$ is propagated in time along a nuclear path $\mathbf{R}_{Kk}(t)$, which is not necessarily a classical trajectory. Naturally the nuclear wavepacket $\chi_{Kk}(\mathbf{R}-\mathbf{R}_{Kk}(t),t)$ is also generated around the center $\mathbf{R}_{Kk}(t)$. Both of them are affected by laser fields and nonadiabatic interactions. We study below how the nonadiabatically coupled electronic and nuclear wavepackets should be propagated in time under laser fields.

A. Mixed quantum-classical Hamiltonian in an optical field

We begin with a general theory for mixed quantum-classical representation of dynamics in a system composed of fast and slow subsystems in which the former and latter are respectively treated quantum and classical mechanically. In the present case, the fast and slow subsystems happen to be electronic and nuclear parts, respectively.

We start from the following full quantum mechanical molecular Hamiltonian in an optical field having the vector potential $\mathbf{A}$,

$$\mathcal{H}(\mathbf{r},\mathbf{R}|\mathbf{A}) = \frac{1}{2}\sum_{k=1}^{3N_n}\left(\hat{P}_k - \frac{Z_k e}{c}A_k(\mathbf{R})\right)^2 + \mathcal{H}^{(\mathrm{el})}(\mathbf{r};\mathbf{R}|\mathbf{A}), \quad (3)$$

with $\mathcal{H}^{(\mathrm{el})}(\mathbf{r};\mathbf{R}|\mathbf{A})$ being the electronic Hamiltonian under the electromagnetic field

$$\mathcal{H}^{(\mathrm{el})}(\mathbf{r};\mathbf{R}|\mathbf{A}) = \frac{1}{2}\sum_{j=1}^{3N_e}\left(\hat{p}_j + \frac{e}{c}A_j(\mathbf{r})\right)^2 + V_c(\mathbf{r};\mathbf{R}), \quad (4)$$

where V_c collectively denotes the Coulombic interactions of electron-electron, electron-nuclei, and nuclei-nuclei. $A_k(\mathbf{R})$ and $A_j(\mathbf{r})$ are the vector potentials for nuclei and electrons, respectively. N_e and N_n are the number of electrons and nuclei, respectively, included in a molecule. Throughout this section, we use the mass-weighted coordinates in which all the masses are scaled to unity. Here, $\mathbf{R}=\{R_k|k=1,\cdots,3N_n\}$ is the collective vector of all the nuclear positions with $\hat{\mathbf{P}}=\{\hat{P}_k|k=1,\cdots,3N_n\}$ being the vector of associated momenta. $Z_k e$ and c are the nuclear charge and the light velocity, respectively, with $-e$ being the electron charge. The hat as in $\hat{P}$ and so on denotes the quantum operators.

In the present theoretical scheme, the Hamiltonian of Eq. (3), which is represented in configuration space $\{\mathbf{r},\mathbf{R}\}$, is re-expressed in the electronic Hilbert space and nuclear configuration space, whose basis is $\{|\Phi_I(\mathbf{R})\rangle|\mathbf{R}\rangle\}$ such that[7,42]

$$\mathcal{H}(\mathbf{R},\mathrm{elec},\mathbf{A}) \equiv \frac{1}{2}\sum_k\left\{\hat{P}_k - \frac{Z_k e}{c}A_k - i\hbar\sum_{IJ}|\Phi_I\rangle X_{IJ}^k\langle\Phi_J|\right\}^2 + \sum_{IJ}|\Phi_I\rangle\mathcal{H}_{IJ}^{(\mathrm{el})}\langle\Phi_J|, \quad (5)$$

where $X_{IJ}^k \equiv \langle\Phi_I|(\partial/\partial R_k)\Phi_J\rangle$ and $\mathcal{H}_{IJ}^{(\mathrm{el})} \equiv \langle\Phi_I|\mathcal{H}^{(\mathrm{el})}(\mathbf{r};\mathbf{R}|\mathbf{A})|\Phi_J\rangle$. This Hamiltonian manifests a parallelism between the electromagnetic effects and nonadiabatic coupling. Here, we only mention the Aharonov–Bohm effect[43] and the Longuet–Higgins[44] (or Berry[45]) phase. Also, a Lorentz-force-like term arising from the nonadiabatic coupling has been briefly discussed in Ref. 7. To attain a mixed quantum-classical representation, we classicalize the above Hamiltonian (5) so as to be accessible to its (approximate) solutions more easily by simply changing the nuclear momentum operator $\hat{P}_k$ in $\mathcal{H}(\mathbf{R},\mathrm{elec},\mathbf{A})$ to its classical counterpart P_k such that

$$\tilde{\mathcal{H}}(\mathbf{R},\mathbf{P},\mathrm{elec},\mathbf{A}) \equiv \frac{1}{2}\sum_k\left(P_k - \frac{Z_k e}{c}A_k - i\hbar\sum_{IJ}|\Phi_I\rangle X_{IJ}^k\langle\Phi_J|\right)^2 + \sum_{IJ}|\Phi_I\rangle\mathcal{H}_{IJ}^{(\mathrm{el})}\langle\Phi_J|. \quad (6)$$

The tilde over $\mathcal{H}(\mathbf{R},\mathbf{P},\mathrm{elec},\mathbf{A})$ indicates such a mixed quantum-classical representation.

B. Coupled dynamics of electrons and nuclei

The dynamical equations of motion for electron wavepacket are derived in terms of the time-dependent variational principle subject to

$$\delta\int dt\langle\Phi(\mathbf{R},t)|\left(i\hbar\frac{\partial}{\partial t} - \tilde{\mathcal{H}}(\mathbf{R},\mathbf{P},\mathrm{elec},\mathbf{A})\right)|\Phi(\mathbf{R},t)\rangle = 0, \quad (7)$$

where $\tilde{\mathcal{H}}(\mathbf{R},\mathbf{P},\mathrm{elec},\mathbf{A})$ are the total Hamiltonian defined in Eq. (6). As usual, we expand the electronic wavepacket as

$$\Phi(\mathbf{r},t;\mathbf{R}(t)) = \sum_I C_I(t)\Phi_I(\mathbf{r};\mathbf{R})|_{\mathbf{R}=\mathbf{R}(t)}, \quad (8)$$

where $\{\Phi_I(\mathbf{r};\mathbf{R})\}$ are basis functions such as the Slater determinants generated at each nuclear position $\mathbf{R}$, and thereby the electronic dynamics is cast into the associated coefficients $\{C_I(t)\}$. Taking account of the right variation as well as the left variation in Eq. (7), we obtain the coupled equations for the electron dynamics as

$$i\hbar\frac{\partial}{\partial t}C_I = \sum_J\left[\mathcal{H}_{IJ}^{(\mathrm{el})} - i\hbar\sum_k\left(P_k - \frac{Z_k e}{c}A_k\right)X_{IJ}^k - \frac{\hbar^2}{4}\sum_k(Y_{IJ}^k + Y_{JI}^{k*})\right]C_J. \quad (9)$$

This is the generalization of the electron wavepacket theory to the dynamics in optical field.[42] Note that the second derivative coupling elements, $Y_{IJ}^k \equiv \langle\Phi_I|\partial^2/\partial R_k^2|\Phi_J\rangle$, in this expression has no direct interaction with the external vector potential $\mathbf{A}$, while the first derivative coupling elements X_{IJ}^k directly couple with A_k.

We next establish the nuclear equations of motion. The "Hamilton canonical equations of motion" establish the following set of equations:[34,35,42]

$$\frac{d^2}{dt^2}\mathcal{R}^k = -\sum_{IJ}\frac{\partial}{\partial R_k}(|\Phi_I\rangle\mathcal{H}_{IJ}^{(\mathrm{el})}\langle\Phi_J|) - \frac{Z_k e}{c}\frac{\partial}{\partial t}A_k(\mathbf{R},t) + i\hbar\sum_{IJ}\sum_l\dot{R}_l\left[\frac{\partial}{\partial R_k}(|\Phi_I\rangle X_{IJ}^l\langle\Phi_J|) - \frac{\partial}{\partial R_l}(|\Phi_I\rangle X_{IJ}^k\langle\Phi_J|)\right] + \frac{e}{c}\sum_l\dot{R}_l \times\left(\frac{\partial}{\partial R_k}Z_l A_l - \frac{\partial}{\partial R_l}Z_k A_k\right), \quad (10)$$

which is defined in the joint nuclear $(\mathbf{R},\mathbf{P})$-space and the electronic Hilbert space. Therefore, to use this operator in practice, we should project it to a matrix form by sandwiching two electronic states, say, $\langle\Phi_I|$ and $|\Phi_J\rangle$ as

$$\mathcal{F}_{IJ}^{i_a} \equiv \langle \Phi_I | \ddot{\mathcal{R}}^{i_a} | \Phi_J \rangle = -\sum_K [X_{IK}^{i_a} \mathcal{H}_{KJ}^{(\mathrm{el})} - \mathcal{H}_{IK}^{(\mathrm{el})} X_{KJ}^{i_a}] - \frac{\partial \mathcal{H}_{IJ}^{(\mathrm{el})}}{\partial R_{i_a}} + i\hbar \sum_b^{\mathrm{nuc.}} \sum_{i_b}^{x,y,z} \dot{R}_{i_b} \left[\frac{\partial X_{IJ}^{i_b}}{\partial R_{i_a}} - \frac{\partial X_{IJ}^{i_a}}{\partial R_{i_b}} \right] + Z_a e (\mathbf{E}_a + \dot{\mathbf{R}}_a \times \mathbf{B}_a)_{i_a} \delta_{IJ}, \tag{11}$$

where we have rewritten the suffices such that a and b specify the nuclei and i_b, for instance, specifies one of the (x,y,z) coordinates in the Euclidean space for the nuclei. Equation (11) is a natural generalization of the classical force and is called the force matrix.[34]

In a particular case that

$$X_{\alpha\beta}^k = 0 \quad \text{and} \quad \mathbf{A} = 0, \tag{12}$$

it is most convenient to adopt the adiabatic wave functions $\{\psi_\alpha\}$, satisfying

$$H^{(\mathrm{el})} \psi_\alpha = E_\alpha^{\mathrm{ad}} \psi_\alpha, \tag{13}$$

where $H^{(\mathrm{el})}$ is the field-free electronic Hamiltonian of Eq. (4). Then we have

$$\mathcal{F}_{\alpha\beta}^k = -\delta_{\alpha\beta} \frac{\partial E_\beta^{\mathrm{ad}}}{\partial R_k}, \tag{14}$$

subject to the condition Eq. (12). Therefore the force matrix in the adiabatic limit reproduces the Born–Oppenheimer forces in its diagonal elements.

If a complete electronic basis was available, the first three terms in the rightmost hand of Eq. (11) are combined into a single piece as the Hellman–Feynman force,

$$-\sum_K [X_{IK}^{i_a} \mathcal{H}_{KJ}^{(\mathrm{el})} - \mathcal{H}_{IK}^{(\mathrm{el})} X_{KJ}^{i_a}] - \frac{\partial \mathcal{H}_{IJ}^{(\mathrm{el})}}{\partial R_{i_a}} = \left(\frac{\partial \mathcal{H}^{(\mathrm{el})}}{\partial R_{i_a}} \right)_{IJ}, \tag{15}$$

and furthermore it holds that $(\partial \mathcal{H}^{(\mathrm{el})} / \partial R_{i_a})_{IJ} = (\partial H^{(\mathrm{el})} / \partial R_{i_a})_{IJ}$. Thus the effect of the laser field on the force matrix through the reorganization of the electronic state should be quite limited (actually zero for a complete basis set). Only the classical Lorentz forces working on the nuclei are the dominant contribution to the force matrix.

C. The SET

The field-free SET is readily extended to the case of electron dynamics in laser field within the present theoretical scheme. Going back to the force (acceleration) operator in Eq. (10), we take a simple average of it over an electron wavepacket, represented as in Eq. (8), resulting in

$$\langle \Phi | \ddot{\mathcal{R}}^{i_a} | \Phi \rangle = -\sum_{I,J,K} C_I^* (X_{IK}^{i_a} \mathcal{H}_{KJ}^{(\mathrm{el})} - \mathcal{H}_{IK}^{(\mathrm{el})} X_{KJ}^{i_a}) C_J - \sum_{IJ} C_I^* \frac{\partial \mathcal{H}_{IJ}^{(\mathrm{el})}}{\partial R_{i_a}} C_J + q_a e (\mathbf{E}_a + \dot{\mathbf{R}}_a \times \mathbf{B}_a)_{i_a}. \tag{16}$$

This expression is theoretically valid even for finite bases. However, if a complete basis set was available, this expression was reduced to the form using the Hellmann–Feynman force as

$$\langle \Phi | \ddot{\mathcal{R}}^{i_a} | \Phi \rangle = -\sum_{I,J} C_I^* \left(\frac{\partial \mathcal{H}^{(\mathrm{el})}}{\partial R_{i_a}} \right)_{IJ} C_J + q_a e (\mathbf{E}_a + \dot{\mathbf{R}}_a \times \mathbf{B}_a)_{i_a}. \tag{17}$$

Further, if the optical interaction for electrons is independent of the nuclear coordinates, the Hellmann–Feynman force in Eq. (17) turns out to be free of the optical term such that

$$\langle \Phi | \ddot{\mathcal{R}}^{i_a} | \Phi \rangle = -\sum_{I,J} C_I^* \left(\frac{\partial H^{(\mathrm{el})}}{\partial R_{i_a}} \right)_{IJ} C_J + q_a e (\mathbf{E}_a + \dot{\mathbf{R}}_a \times \mathbf{B}_a)_{i_a}. \tag{18}$$

Of course, these nuclear dynamical equations should be solved simultaneously with the electronic dynamics of Eq. (9), which is slightly rewritten as

$$i\hbar \frac{\partial}{\partial t} C_I = \sum_J \left[\mathcal{H}_{IJ}^{(\mathrm{el})} - i\hbar \sum_k \dot{R}_k X_{IJ}^k + \hbar^2 \sum_k \left(\langle \Phi | \frac{\partial}{\partial R_k} | \Phi \rangle - \frac{1}{4} (Y_{IJ}^k + Y_{JI}^{k*}) \right) \right] C_J. \tag{19}$$

Note that the terms $-(\hbar^2/4)\Sigma_k (Y_{IJ}^k + Y_{JI}^{k*})$ in Eqs. (9) and (19) are not found in the conventional (intuitively derived) SET, but these are often neglected anyway for the reason of the presence of $\hbar^2$.

In SET, the total wave function with an electronic wavepacket launched initially on a path $\mathbf{R}_{Ii}$ (the ith path on an electronic state I) should be represented as

$$\Phi_I(\mathbf{r}; \mathbf{R}(t_{\mathrm{before}})) \delta(\mathbf{R} - \mathbf{R}_{Ii}(t_{\mathrm{before}})) \rightarrow \delta(\mathbf{R} - \langle \mathbf{R} \rangle (t_{\mathrm{after}})) \sum_K^{\mathrm{adiabatic\ PES}} C_K(t_{\mathrm{after}}) \Phi_K(\mathbf{r}; \langle \mathbf{R} \rangle (t_{\mathrm{after}})), \tag{20}$$

where the left hand side denotes the initial wave function before bifurcation, while the right hand one does a linear combination of the branching components after crossing and/or laser shining and $\langle \mathbf{R} \rangle$ denotes a path running on the average potential energy surface.

We have two comments about the property of the SET. (i) It is well known that a path generated in the mean-field in the sense of Eq. (18) is totally unphysical after the passage of a nonadiabatic region such as avoided crossing. Nevertheless, as far as only a single passage is concerned, SET using a single path gives quite an accurate transition probability (see Ref. 35 for numerical examples). This is because the electronic-state mixing is kept taken into account coherently in terms of Eq. (19) all the way through the nonadiabatic interaction region. This makes a marked contrast to the stochastic method such as the *naive* version of the surface hopping model, in which hopping of a trajectory from one potential energy surface to another is to be made locally at some representative points with a given probability. Surface hopping model is therefore very powerful in that it is convenient and easy to implement but in return should require a bunch of many trajectories. Also, the coherence among the

electronic transition amplitudes on the individual hopping trajectories can be destroyed for a coupling element of wide spatial range. (ii) The SET equations in intense laser fields, using Eqs. (16) and (19) without $-(\hbar^2/4)\Sigma_k(Y_{IJ}^k+Y_{JI}^{k*})$, have been applied extensively to chemical dynamics by the present authors.[7,39,42] In particular, the role of the nonadiabatic coupling elements in electronic excitation with infrared lasers has been highlighted.[7]

D. PSANB

Since the generation process of branching paths in a laser field is subtle, we describe it rather precisely.

1. Eigenforces and branching paths

The electronic wavepacket propagates along nuclear paths that are driven by the force matrix. Suppose we have an electronic wavepacket $\Phi(\mathbf{r};\mathbf{R}(t))$ at a phase-space point $(\mathbf{R},\mathbf{P})$. To materialize an electronic-state mixing among given basis functions $\{\Phi_I(\mathbf{r};\mathbf{R})\}$ (either adiabatic or any diabatic basis), we first integrate Eq. (9) for a short time, say, Δt, to give a new set of $\{C_I(t)\}$. Next we want to run a path using the force matrix $\mathcal{F}(\mathbf{R})$ again for a short time Δt. To avoid the additional mixing due to the off-diagonal elements of the force matrix, we diagonalize it at $\mathbf{R}$ such that

$$\mathbf{U}(\mathbf{R})\mathcal{F}(\mathbf{R})\mathbf{U}(\mathbf{R})^{-1}=\begin{pmatrix} f_1(\mathbf{R}) & 0 & \cdots \\ 0 & f_2(\mathbf{R}) & \\ \vdots & & \ddots \end{pmatrix}, \tag{21}$$

with the associated electronic basis-set transformation

$$\mathbf{U}(\mathbf{R})\begin{pmatrix} \Phi_1(\mathbf{r};\mathbf{R}) \\ \Phi_2(\mathbf{r};\mathbf{R}) \\ \vdots \end{pmatrix}=\begin{pmatrix} \lambda_1(\mathbf{r};\mathbf{R}) \\ \lambda_2(\mathbf{r};\mathbf{R}) \\ \vdots \end{pmatrix}. \tag{22}$$

The electronic wavepacket obtained as above may be reexpanded in the eigenfunctions $\{\lambda_K(\mathbf{r};\mathbf{R})\}$ such that

$$\Phi(\mathbf{r};\mathbf{R}(t))=\sum_K D_K(t)\lambda_K(\mathbf{r};\mathbf{R})|_{\mathbf{R}=\mathbf{R}(t)}, \tag{23}$$

so that each electronic component $D_K(t)\lambda_K(\mathbf{r};\mathbf{R})$ can be carried by its own path being driven by the eigenforce f_K to reach a new point after Δt. However, different eigenforces make different paths even if they start from a single phase-space point $(\mathbf{R},\mathbf{P})$ as

$$(\mathbf{R},\mathbf{P})\rightarrow(\mathbf{R}_K,\mathbf{P}_K). \tag{24}$$

Therefore a path at $\mathbf{R}$ is branched to as many pieces as the number of electronic states involved in the nonadiabatic coupling. The electronic-state mixing should be considered again at the individual points $(\mathbf{R}_K,\mathbf{P}_K)$, making the corresponding component $D_K(t)\lambda_K(\mathbf{r};\mathbf{R})$ in Eq. (23) renew to resume the integration of Eq. (9). Hence, the cascade of path branching should continue as long as the nonadiabatic coupling cannot be effectively ignored. This path branching is a general feature of the dynamics of *kinematically* coupled quantum and classical subsystems. The full details of the entire procedure have been summarized elsewhere.[34]

2. Averaging over the paths to extract a (few) representative path(s) in the coupling region

Since the exact and faithful treatment of the above branching procedure leads to a cascade of infinitely many paths, we take the following phase-space averaging of the to-be-branched paths. It is generally anticipated that the fine branching paths should not geometrically deviate much from each other in phase space for a short time propagation. In other words, they should localize along a representative path forming a tubelike structure. Therefore we extract such a representative path by taking an average of phase-space points in the following manner.

(i) Suppose we have a path ending at $(\langle\mathbf{R}(t)\rangle,\langle\mathbf{P}(t)\rangle)$ in phase space. At this point, diagonalize the force matrix,

$$\mathcal{F}(\langle\mathbf{R}\rangle)|\lambda_K(\langle\mathbf{R}\rangle)\rangle=|\lambda_K(\langle\mathbf{R}\rangle)\rangle f_K(\langle\mathbf{R}\rangle), \tag{25}$$

to obtain the eigenforces $\{f_K\}$ and its eigenstates $\{|\lambda_K\rangle\}$. The wavepacket $\Phi(\mathbf{r};\langle\mathbf{R}(t)\rangle)$ is expanded in terms of these eigenstates as in Eq. (23).

(ii) The Kth eigenforce drives a path starting from $(\langle\mathbf{R}(t)\rangle,\langle\mathbf{P}(t)\rangle)$ for a short time Δt in terms of the Hamilton canonical equations of motion as

$$\mathbf{R}_K(t+\Delta t)=\langle\mathbf{R}(t)\rangle+\Delta\mathbf{R}_K, \tag{26}$$

$$\mathbf{P}_K(t+\Delta t)=\langle\mathbf{P}(t)\rangle+\Delta\mathbf{P}_K. \tag{27}$$

(iii) Average them into the form

$$\langle\mathbf{R}(t+\Delta t)\rangle=\langle\mathbf{R}(t)\rangle+\sum_K|D_K(t)|^2\Delta\mathbf{R}_K, \tag{28}$$

$$\langle\mathbf{P}(t+\Delta t)\rangle=\langle\mathbf{P}(t)\rangle+\sum_K|D_K(t)|^2\Delta\mathbf{P}_K, \tag{29}$$

which makes the next point $(\langle\mathbf{R}(t+\Delta t)\rangle,\langle\mathbf{P}(t+\Delta t)\rangle)$ of the representative path.

(iv) With this averaged point, we calculate

$$\mathcal{F}(\langle\mathbf{R}(t+\Delta t)\rangle)|\lambda_K(\langle\mathbf{R}(t+\Delta t)\rangle)\rangle$$
$$=|\lambda_K(\langle\mathbf{R}(t+\Delta t)\rangle)\rangle f_K(\langle\mathbf{R}(t+\Delta t)\rangle) \tag{30}$$

and return anew to the step (ii). The successive applications of procedures (i)–(iii) give a single finite path.

Path generation using the above averaging procedure should be performed simultaneously with the coherent electronic wavepacket mixing through Eq. (9). Also, the force matrix in Eq. (25) and the weighting factors $|D_K(t)|^2$ are to be renewed in the repeated use of them as the path and electronic wavepackets are evolved in time. Therefore, as in SET (see Sec. II C), the coherence among the electronic transition amplitudes is retained during the above process.

3. Branching of the averaged path

Let us stop the averaging procedure at a point, which can be an exit point of the interaction region or even an inner position in the coupling region. Suppose we are tracking one

of the averaged paths, say, the Kth path, $(\mathbf{R}_K(t),\mathbf{P}_K(t))$. To emphasize that every force is generated along this path, we rewrite Eq. (21) explicitly as

$$\mathbf{U}(\mathbf{R}_K)\mathcal{F}(\mathbf{R}_K)\mathbf{U}(\mathbf{R}_K)^{-1}=\begin{pmatrix} f_1(\mathbf{R}_K) & 0 & \cdots \\ 0 & f_2(\mathbf{R}_K) & \\ \vdots & & \ddots \end{pmatrix}, \tag{31}$$

where the dependence of the force matrix on $\mathbf{R}_K$ has been stressed. The right hand side of this representation reminds that other eigenforces, say, f_L, are also calculated along $\mathbf{R}_K(t)$. Therefore, at a point on the path $(\mathbf{R}_K(t),\mathbf{P}_K(t))$, one may switch the force from f_K to f_L to emanate *another* path such that $(\mathbf{R}_K(t),\mathbf{P}_K(t))\rightarrow(\mathbf{R}_L(t+\Delta t),\mathbf{P}_L(t+\Delta t))$ driven by f_L. If one uses f_K at the same point, it follows that $(\mathbf{R}_K(t),\mathbf{P}_K(t))\rightarrow(\mathbf{R}_K(t+\Delta t),\mathbf{P}_K(t+\Delta t))$. Thus this procedure allows that a path can naturally branch as soon as the averaging is terminated. These are the paths of the first generation of branching.

The individual branched paths of the first generation may resume the averaging to the next branching points, which gives rise to the second generation, and then may undergo further branching if these are embedded in a strong interaction region. Or if the path comes to an exit point of the nonadiabatic and/or optical interactions, beyond which the coupling is effectively vanished, the mixing of electronic states is switched off, and we stop taking the average as in Eqs. (28) and (29) and let the every individual component

$$D_K(t)\lambda_K(\mathbf{r};\mathbf{R}_K(t)) \tag{32}$$

run being driven by its own force, which comes from the gradient of each potential energy surface. Then the coefficients $D_K(t)$ coherently carry the information of transition amplitudes. After the final branching at the exit point, electronic-state mixing does not occur any longer.

The method presented in this section is referred to as PSANB.[35] Since an electronic wavepacket, launched initially on a path $\mathbf{R}_{Ii}$ (the ith path on an electronic state I) undergoes bifurcation and mixing, the propagation of the total wave function (before quantization of nuclear paths) should be represented as

$$\begin{aligned}&\Phi_I(\mathbf{r};\mathbf{R}(t_{\text{before}}))\delta(\mathbf{R}-\mathbf{R}_{Ii}(t_{\text{before}}))\\ &\rightarrow \sum_{K}^{\text{adiabatic PES on } K}\sum_{k} C_{Kk}(t_{\text{after}})\Phi_K(\mathbf{r};\mathbf{R}_{Kk}(t_{\text{after}}))\\ &\quad\times\delta(\mathbf{R}-\mathbf{R}_{Kk}(t_{\text{after}})),\end{aligned} \tag{33}$$

which should be compared with the SET propagation of Eq. (20).

To summarize, PSANB is similar to the SET in that the coherent electronic-state mixing is performed along a path, and hence only a few paths are needed to reproduce an accurate transition probability in contrast to the (primitive) surface hopping trajectories. On the other hand, PSANB and SET are different in that (i) the averaging to give such a non-Born–Oppenheimer path (nonclassical trajectory) is made over the force (SET) or performed over the phase-space positions of to-be-branching paths (PSANB) and, more importantly, (ii) those non-Born–Oppenheimer paths cannot bifurcate and keep running on an average potential (SET) or can bifurcate as many times as one designates and eventually converge to classical trajectories after all the nonadiabatic and optical couplings are nullified (PSANB).

III. QUANTIZATION OF NUCLEAR PATHS WITH WAVEPACKETS

So far, we have established a method to propagate electronic wavepackets along branching non-Born–Oppenheimer path under a classical vector field. Upon comparing Eqs. (33) and (2), it is natural to set our next target to quantization of those nuclear paths by associating them with nuclear wavepackets. To do so, we use our developed semiclassical wave function called the ADF.[36] Among many possibilities to apply this theory, we particularly choose the NVG, a semiclassical Gaussian approximation to ADF. A theoretical advantage of ADF-NVG is that it can be applied to nonclassical paths, and indeed, we have shown before how it works in field-free nonadiabatic dynamics.[35] We therefore want to apply the ADF-NVG method to the present case and study an extension of this theory to dynamics under laser field. We outline below a proof that the equation of motion for ADF remains in the same form even if a classical vector potential exists.

A. ADF equation of motion in laser field

We study the following nonrelativistic Schrödinger equation:

$$i\hbar\frac{\partial}{\partial t}\chi(\mathbf{R},t)=\left[\frac{1}{2}\sum_k\frac{1}{m_k}\left(\hat{P}_k-\frac{Z_k e}{c}A_k(\mathbf{R})\right)^2+V(\mathbf{R})\right]\chi(\mathbf{R},t), \tag{34}$$

where $\hat{P}_k$ is the quantum momentum operator,

$$\hat{P}_k=\frac{\hbar}{i}\frac{\partial}{\partial R_k}, \tag{35}$$

and should be distinguished from its classical canonical momentum P_k. Here again, we resort to the mass-weighted coordinates, rescaling all the masses to

$$m_k=1. \tag{36}$$

The velocity of a particle is correlated with its momentum in such a way that

$$v_k=P_k-\frac{Z_k e}{c}A_k. \tag{37}$$

The classical counterpart of this dynamics is represented in the following Hamilton–Jacobi equation:

$$\frac{\partial}{\partial t}S(\mathbf{R},t)+\frac{1}{2}\sum_k\left(\frac{\partial S(\mathbf{R},t)}{\partial R_k}-\frac{Z_k e}{c}A_k\right)^2+V(\mathbf{R})=0, \tag{38}$$

where the momentum is generated through the action integral as

$$P_k = \frac{\partial S(\mathbf{R},t)}{\partial R_k}. \tag{39}$$

It is convenient to summarize the classical relations as

$$\left(\frac{\partial S(\mathbf{R},t)}{\partial R_k} - \frac{Z_k e}{c}A_k\right) = v_k = P_k - \frac{Z_k e}{c}A_k \tag{40}$$

subject to the condition Eq. (36).

We set the total wave function in the form of

$$\chi(\mathbf{R},t) = \exp\left(\frac{i}{\hbar}S(\mathbf{R},t)\right)F(\mathbf{R},t). \tag{41}$$

The left hand side of the Schrödinger equation is

$$i\hbar\frac{\partial\chi(\mathbf{R},t)}{\partial t} = \exp\left(\frac{i}{\hbar}S(\mathbf{R},t)\right)\left(-\frac{\partial S}{\partial t}F + i\hbar\frac{\partial F(\mathbf{R},t)}{\partial t}\right). \tag{42}$$

Next, we evaluate the right hand side of Eq. (34). Since the kinetic energy parts are somewhat cumbersome, we should treat them with some care. First, we examine the operations on $\exp((i/\hbar)S)$ as

$$\left(\hat{P}_k - \frac{Z_k e}{c}A_k(\mathbf{R})\right)\exp\left(\frac{i}{\hbar}S\right) = \exp\left(\frac{i}{\hbar}S\right)\left(P_k - \frac{Z_k e}{c}A_k(\mathbf{R})\right) \tag{43}$$

and

$$\begin{aligned}
&\frac{1}{2}\left(\hat{P}_k - \frac{Z_k e}{c}A_k(\mathbf{R})\right)^2\exp\left(\frac{i}{\hbar}S\right)\\
&\quad= \frac{1}{2}\left(\hat{P}_k - \frac{Z_k e}{c}A_k(\mathbf{R})\right)\left(P_k - \frac{Z_k e}{c}A_k(\mathbf{R})\right)\exp\left(\frac{i}{\hbar}S\right)\\
&\quad= \frac{1}{2}\exp\left(\frac{i}{\hbar}S\right)\left[\left(P_k - \frac{Z_k e}{c}A_k(\mathbf{R})\right)^2\right.\\
&\qquad\left.+\hat{P}_k\left(P_k - \frac{Z_k e}{c}A_k(\mathbf{R})\right)\right].
\end{aligned} \tag{44}$$

Then the straightforward formulation goes as follows:

$$\begin{aligned}
&\left[\frac{1}{2}\sum_k\left(\hat{P}_k - \frac{Z_k e}{c}A_k\right)^2 + V(\mathbf{R})\right]\exp\left(\frac{i}{\hbar}S(\mathbf{R},\mathbf{t})\right)F(\mathbf{R},\mathbf{t})\\
&\quad= F\exp\left(\frac{i}{\hbar}S\right)\left\{\sum_k\left[\frac{1}{2}\left(P_k - \frac{Z_k e}{c}A_k\right)^2\right.\right.\\
&\qquad\left.\left.+\frac{1}{2}\hat{P}_k\left(P_k - \frac{Z_k e}{c}A_k\right)\right] + V(\mathbf{R})\right\} + \exp\left(\frac{i}{\hbar}S\right)\frac{1}{2}\sum_k\hat{P}_k^2F\\
&\qquad+\exp\left(\frac{i}{\hbar}S\right)\sum_k\left(P_k - \frac{Z_k e}{c}A_k\right)[\hat{P}_k F].
\end{aligned} \tag{45}$$

Combining Eqs. (42) and (45), we see

$$\begin{aligned}
-\frac{\partial S}{\partial t}F + i\hbar\frac{\partial F}{\partial t} &= F\left\{\sum_k\left[\frac{1}{2}\left(P_k - \frac{Z_k e}{c}A_k\right)^2\right.\right.\\
&\quad\left.\left.+\frac{1}{2}\hat{P}_k\left(P_k - \frac{Z_k e}{c}A_k\right)\right] + V(\mathbf{R})\right\}\\
&\quad+\frac{1}{2}\sum_k\hat{P}_k^2F + \sum_k\left(P_k - \frac{Z_k e}{c}A_k\right)[\hat{P}_k F].
\end{aligned}$$

With the help of the Hamilton–Jacobi equation (38), we have [using Eq. (36)]

$$\frac{\partial F(\mathbf{R},t)}{\partial t} = \left[-\mathbf{v}\cdot\nabla - \frac{1}{2}[\nabla\cdot\mathbf{v}] + \frac{i}{2}\hbar\nabla^2\right]F. \tag{46}$$

Note that this ADF equation is of exactly the same form as that for field-free case. This is not surprising since the ADF equation essentially represents kinematics. Therefore, the technique developed before for (approximately) solving the ADF equation in nonadiabatic problem can be readily applied to nonadiabatic dynamics in laser field.

B. ADF-NVG

The ADF equation, Eq. (46), may be transformed into an integral form such that

$$\begin{aligned}
&F(\mathbf{R}-\mathbf{R}(t+\Delta t),t+\Delta t)\\
&\quad= \exp\left[\Delta t\left(-\frac{1}{2}\vec{\nabla}\cdot\vec{v} + \frac{i\hbar}{2}\vec{\nabla}^2\right)\right]F(\mathbf{R}-\mathbf{R}(t),t),
\end{aligned} \tag{47}$$

to which one can apply the so-called Trotter decomposition. We approximate $F(\mathbf{R}-\mathbf{R}(t),t)$ in terms of the Gaussian function

$$\begin{aligned}
F(\mathbf{R}-\mathbf{R}(t),t) &= \pi^{-N/4}[\det(\mathbf{\Gamma}+\mathbf{\Gamma}^*)]^{1/4}\\
&\quad\times\exp[-(\mathbf{R}-\mathbf{R}(t))^T\mathbf{\Gamma}(t)(\mathbf{R}-\mathbf{R}(t))].
\end{aligned} \tag{48}$$

It has been found that the Gaussian of the inverse exponent

$$\mathbf{\Gamma}(t) = \frac{1}{\mathbf{C}(t) + i\mathbf{D}(t)} \tag{49}$$

is particularly useful since the time evolutions of $\mathbf{C}(t)$ and $\mathbf{D}(t)$ are given explicitly as

$$\mathbf{C}(t+\Delta t) = \exp\left(\int_t^{t+\Delta t}\mathbf{\Omega}dt\right)\mathbf{C}(t)\exp\left(\int_t^{t+\Delta t}\mathbf{\Omega}dt\right) \tag{50}$$

and

$$\mathbf{D}(t+\Delta t) = \exp\left(\int_t^{t+\Delta t}\mathbf{\Omega}dt\right)\mathbf{D}(t)\exp\left(\int_t^{t+\Delta t}\mathbf{\Omega}dt\right) + 2\hbar i\Delta t\mathbf{I}, \tag{51}$$

respectively, and $\mathbf{\Omega}$ is a matrix defined as

$$\mathbf{\Omega}_{kl}(t) = \frac{\partial^2 S}{\partial R_k\,\partial R_l} \tag{52}$$

at a trajectory point $\mathbf{R}(t)$. Also, the differential equations for them are given as

$$\dot{\mathbf{C}}(t) = \mathbf{\Omega}(t)\mathbf{C}(t) + \mathbf{C}(t)\mathbf{\Omega}(t) \tag{53}$$

and

$$\dot{\mathbf{D}}(t) = \mathbf{\Omega}(t)\mathbf{D}(t) + \mathbf{D}(t)\mathbf{\Omega}(t) + 2\hbar i\mathbf{I}. \tag{54}$$

The exponent $\mathbf{C}(t)$ is responsible for describing only the velocity gradient, $-\frac{1}{2}\vec{\nabla}\cdot\vec{v}$ in Eq. (47), while $\mathbf{D}(t)$ reflects the dynamics not only for the velocity gradient but also, arising from the quantum diffusion term, $(i\hbar/2)\vec{\nabla}^2$ of Eq. (47). The Planck constant appears only in the quantum diffusion term, and therefore only $\mathbf{D}(t)$ is to be scaled to the magnitude of $\hbar$. The details of this theory is reported elsewhere.[46]

With these wavepackets generated for nuclear paths along with the electronic wave functions obtained as above, we finally attain a total wave function in the form of Eq. (2), which is quantum electronic and nuclear wavepackets propagated within an on-the-fly scheme. Note in this representation that it is possible to use as many NVGs as one can to represent a global nuclear wave function on each nuclear path for the higher approximation. Nevertheless, as we show later numerically, even the single Gaussian approximation applied to individual branching path provides already remarkably good results. In the ADF-NVG scheme, the phase information, up to the Maslov phase, is correctly taken into account.

C. The total electronic and nuclear wave function

Accumulating all the dynamical components as constructed above, we can build a total electronic and nuclear wavepackets along the non-Born–Oppenheimer paths as

$$\Psi^{\mathrm{tot}}_{\mathrm{OTF}}(\mathbf{r},\mathbf{R},t) = \sum_{K}^{\mathrm{state}}\sum_{k}^{\mathrm{path}} \Phi_K(\mathbf{r},t;\mathbf{R}_{Kk}(t))C_{Kk}(t) \times F_{\mathrm{NVG}}(\mathbf{R}-\mathbf{R}_{Kk}(t),t)\exp\left[\frac{i}{\hbar}S(\mathbf{R}-\mathbf{R}_{Kk}(t))\right], \tag{55}$$

where the suffix OTF stands for on-the-fly. This representation of the total wave function is made in a little different way of the standard one, which is given as in Eq. (1). Let it be rewritten as

$$\Psi^{\mathrm{tot}}_{\mathrm{QM}}(\mathbf{r},\mathbf{R},t) = \sum_{K}^{\mathrm{state}} \Phi(\mathbf{r},t;\mathbf{R})\chi^{\mathrm{QM}}_K(\mathbf{R},t) \tag{56}$$

for comparison. Then it is clear that rigorous comparison between these wave functions is required to be made in the $(\mathbf{r},\mathbf{R})$ space, even if we use the common electronic basis functions. To avoid such a numerically tedious task, we rewrite our represented wave function of Eq. (55) by assuming that $F_{\mathrm{NVG}}(\mathbf{R}-\mathbf{R}_{Kk}(t),t)$ is spatially well localized, which allows us to approximate $\Psi^{\mathrm{tot}}_{\mathrm{OTF}}(\mathbf{r},\mathbf{R},t)$ as

$$\Psi^{\mathrm{tot}}_{\mathrm{OTF}}(\mathbf{r},\mathbf{R},t) \cong \sum_{K}^{\mathrm{state}} \Phi_K(\mathbf{r},t;\mathbf{R})\sum_{k}^{\mathrm{path}} C_{Kk}(t) \times F_{\mathrm{NVG}}(\mathbf{R}-\mathbf{R}_{Kk}(t),t)\exp\left[\frac{i}{\hbar}S(\mathbf{R}-\mathbf{R}_{Kk}(t))\right] = \sum_{K}^{\mathrm{state}} \Phi_K(\mathbf{r},t;\mathbf{R})\chi^{\mathrm{OTF}}_K(\mathbf{R},t), \tag{57}$$

with an obvious definition

$$\chi^{\mathrm{OTF}}_K(\mathbf{R},t) = \sum_{k}^{\mathrm{path}} C_{Kk}(t)F_{\mathrm{NVG}}(\mathbf{R}-\mathbf{R}_{Kk}(t),t) \times \exp\left[\frac{i}{\hbar}S(\mathbf{R}-\mathbf{R}_{Kk}(t))\right]. \tag{58}$$

Now it is possible to compare it with the quantum mechanical counterpart, $\chi^{\mathrm{QM}}_K(\mathbf{R},t)$. Recall that $C_{Kk}(t)'s$ included in the nuclear wavepacket $\chi^{\mathrm{OTF}}_K(\mathbf{R},t)$ of Eq. (58) have originally emerged from the electronic wavepacket bifurcation along the branching paths.

To find the probability of a state in an electronic state K after the nonadiabatic transition at time t and the nuclear configuration $\mathbf{R}$, we need to calculate

$$|\chi^{\mathrm{OTF}}_K(\mathbf{R},t)|^2. \tag{59}$$

A simple approximation to estimate a probability for a state to be found in the electronic state K at time t is a decoherent sum,

$$P^{\mathrm{dec}}_K(t) = \sum_{k}^{\mathrm{path\ on}\ K} |C_{Kk}(t)|^2. \tag{60}$$

This expression should be most appropriate if a rapid decoherence among nuclear wavepackets is expected. In the present computational scheme, each electronic wavepacket is propagated along the individual paths, and the effect of quantization of nuclear paths in terms of ADF-NVG is not fed back to the electronic dynamics. Therefore, the electronic wavepackets become quickly independent after the nonadiabatic interaction is switched off. In a case where a large nuclear overlap between different electronic states during dynamics exists, the coherent summation may be preferable. In the next section, we apply Eq. (60) to estimate the transition probability.

IV. NUMERICAL STUDIES

We here study the practical implementation of the method. We first survey, using a simple and clear nonadiabatic model system, how the PSANB-ADF-NVG method can work in case with an intense laser field and what kind of difficulty may arise to be overcome. Then, we present an illustrative example of *ab initio* non-Born–Oppenheimer chemistry in terms of HF molecule, suggesting that the method is indeed promising as a practical method.

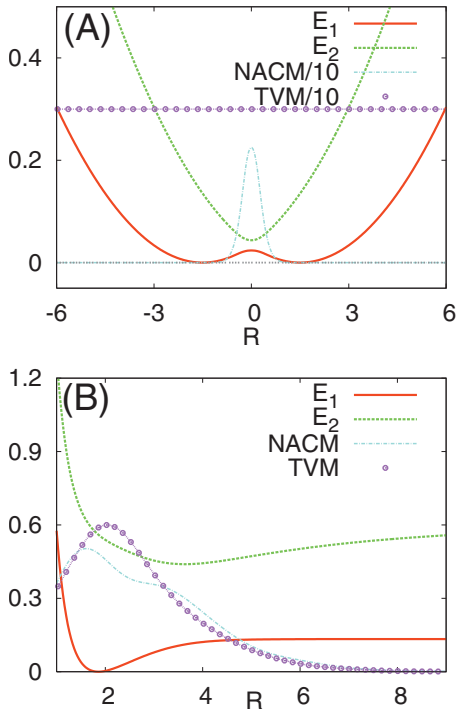

FIG. 1. Energy profiles and the relevant coupling elements vs internuclear distance (in atomic units). (a) A model system (DWL system) and (b) HF molecule. Two adiabatic potential energy curves (E_1 and E_2), nonadiabatic coupling element, and TVM are presented.

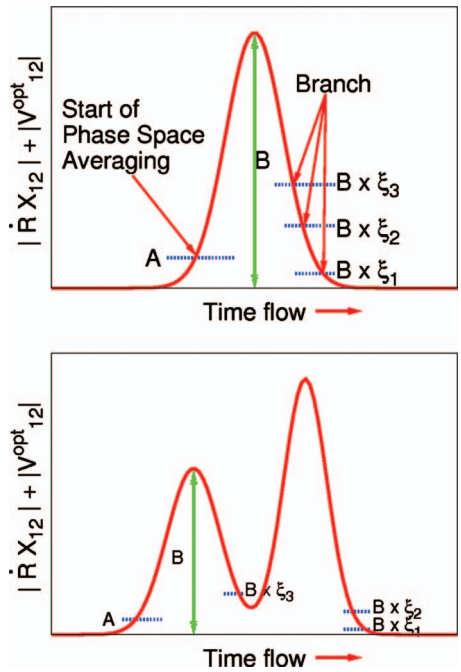

FIG. 2. Two typical patterns of the relative presence of the elements of nonadiabatic coupling ($|\dot{R}X_{12}|$) and optical coupling ($|V_{12}^{\mathrm{opt}}|$) elements. In the upper panel, two couplings deeply overlap and practically only one function is seen. By contrast, two couplings are well separated from each other in the lower panel. In the latter case, a single branching only at the final exit may not suffice to generate appropriate paths.

A. System and practices

1. A model nonadiabatic system under pulse lasers

The first system we study is a two-level system as represented in Fig. 1(a). The two adiabatic potential functions are built up as $W_{2/1}(R)=\frac{1}{2}\{V_{11}-V_{22}\pm\sqrt{(V_{11}-V_{22})^2+4V_c^2}\}$, where $V_{11}=\gamma(R+\alpha)^2$, $V_{22}=\gamma(R-\alpha)^2$, and $V_c=\eta\exp(-\beta x^2)$ with $\alpha=1.5$, $\beta=5.0$, $\gamma=0.015$, and $\eta=0.01$. The off-diagonal elements of the transition dipole matrix, $D_{12}=-D_{21}$, were set to 3. The nonadiabatic coupling elements $X_{12}=-X_{21}$ were obtained from the relation $X_{12}=\Sigma_{i,j}U_{i1}(\partial_R V_{ij})U_{j2}/(W_2-W_1)$, where U is a unitary matrix, which diagonalizes the potential matrix V to a diagonal eigenvalue matrix W. As seen in the figure, the ground state potential surface has a double minimum with the nonadiabatic coupling element spreading over the top of the barrier. We refer to this system as DWL in what follows. The electronic transition velocity moment (TVM) was set to a constant. The effective mass (or reduced mass) was determined to be 1818.18 a.u.

The vector potential of a laser field takes the following general form:

$$A(t)=A_1 f(t;t_{c1},t_{w1})\cos(\omega_1(t-t_{c1})+\delta_1)+A_2 f(t;t_{c2},t_{w2})\cos(\omega_2(t-t_{c2})+\delta_2), \tag{61}$$

the direction of which is set on the molecular axis. ω means a central field frequency, and δ is a carrier envelope phase. The envelope function is defined by $f(t;t_c,t_w)\equiv\exp(-((t-t_c)/t_w)^2)$, where t_c stands for a field peak time and t_w for a typical Gaussian decay time.

2. Computations of branching paths and NVG

In this work we need to generate branching paths (actually PSANB paths) in classical vector field along with the nonadiabatic coupling field, the systematic algorithm for which has to be installed. On the other hand, some essential practice to automatically generate PSANB paths without laser field has been presented elsewhere.[35] Also, we have developed the SET in classical vector fields.[42] Therefore only a new feature of the technical aspects, which arise only from the coexistence of optical and nonadiabatic couplings, will be discussed. Let $V_{12}^{\mathrm{opt}}(t)$ be the optical interaction between the two adiabatic states, whose explicit form is shown in Eq. (A2) in Appendix A, and let $\dot{R}X_{12}$ be the nonadiabatic coupling. Both of these interactions work collectively as a time-dependent coupling element. For a later convenience in describing the path branching, we define

$$\|V(t)\|=|V_{12}^{\mathrm{opt}}(t)|+|\dot{R}X_{12}|. \tag{62}$$

Some typical feature of $\|V(t)\|$ is illustrated in Fig. 2.

In solving the coupled dynamics of PSANB with electronic wavepacket bifurcation, the time step to integrate the equations of motion for nuclei was set to 0.5 a.u. in the sixth order symplectic integrator.[47] Time-evolution of the electronic wave functions was performed with the Chebyshev polynomial expansion method.[48] At each time step to integrate the nuclear dynamics, we reset the electronic Hamiltonian matrix at the renewed nuclear positions.

We then quantize thus obtained PSANB paths in terms of ADF-NVG, the basic practice for one-dimensional of which has been described elsewhere.[35] We here should add a

newly arising matter, that is, how to evaluate the action integral under a laser field, since the PSANB paths we handle are not classical trajectories. To describe a spatial broadening of the action integral for covering the range of the Gaussian function (NVG), we expand the action integral in Eq. (41) up to the second order around the center of NVG, $\mathbf{R}(t)$ as

$$S(\mathbf{R},t;\mathbf{R}(t)) \approx S|_{\mathbf{R}=\mathbf{R}(t)} + \sum_i (R_i - R_i(t)) \left.\frac{\partial S}{\partial R_i}\right|_{\mathbf{R}=\mathbf{R}(t)} + \frac{1}{2}\sum_i \sum_j (R_i - R_i(t)) \times (R_j - R_j(t)) \left.\frac{\partial^2 S}{\partial R_i \partial R_j}\right|_{\mathbf{R}=\mathbf{R}(t)}, \quad (63)$$

where the classical action takes the form as an action integral

$$S = \int dt \left\{ \frac{1}{2} m\dot{\mathbf{R}}^2 - \left(V - \frac{Ze}{c}\mathbf{A}\cdot\dot{\mathbf{R}} \right) \right\}. \quad (64)$$

Then, the first derivative of action at trajectory point is written as

$$\left.\frac{\partial S}{\partial R_i}\right|_{\mathbf{R}=\mathbf{R}(t)} = P_i(t) = m\dot{R}_i + \frac{Ze}{c}A_i(t), \quad (65)$$

and the second derivative is

$$\left.\frac{\partial^2 S}{\partial R_i \partial R_j}\right|_{\mathbf{R}=\mathbf{R}(t)} = \left.\frac{\partial P_j}{\partial R_i}\right|_{\mathbf{R}=\mathbf{R}(t)} = \frac{\dot{P}_j(t)}{\dot{R}_i(t)} = \frac{m\ddot{R}_j(t) + \frac{Ze}{c}\dot{A}_j(t)}{\dot{R}_i(t)}. \quad (66)$$

Note that $\nabla\cdot\mathbf{A}=0$ is applied automatically.

3. Full quantum treatment for comparison

To prepare a set of reference data for comparison, we have performed full quantum mechanical calculations with a one-dimensional reduction of nonadiabatic and optical coupling elements, the details of which are described in Appendix A. The time propagation of multistate coupled nuclear wave function has been performed with use of the Chebyshev expansion method.[48] Time step dt was set to 0.5 a.u., and total propagation times were 1200 and 600 for DWL model and HF molecule, respectively. We have confirmed the convergence of the transition probability by halving the time step. The derivative operator and position operator was treated in a sinc discrete variable representation[49] with 600 grid points uniformly distributed from $R=-10$ to 10 bohrs. We have checked the convergence of the results with respect to the spatial density of grid points. The initial position and momentum are set to 4.0 Bohrs and -30 a.u., respectively. These initial conditions are common to all the examples examined below.

We first display in Fig. 3 the snapshots of the reference wavepackets without laser field to give an idea on their positions at a given time and how the wavepacket branching takes place. For instance, we notice that in this field-free dynamics, the wavepacket experiences a transition around

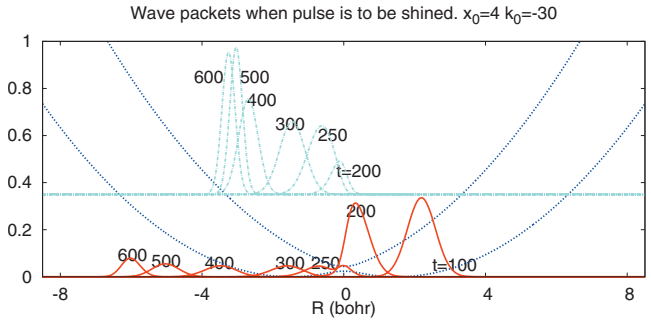

FIG. 3. Time propagation of full quantum wavepackets in the DWL system without laser. Snapshots of the square modulus of the nuclear wavepacket on the ground (red) and excited (blue) states are shown at selected instants. The central position and wave number of the initial wavepacket starting on the ground state are 4.0 and -30 a.u., respectively. Energy gaps at $R=1.5$ and -3.2 bohrs are 0.135 and 0.29 a.u., respectively. After the first passage of the nonadiabatic region, approximately 0.84 of the total population is transferred to the excited state.

$t=200$, and most of its portion (approximately 0.84) is transferred to the excited state. With this global view of the wavepackets, we apply a pulse laser at various timings.

B. Basic feature of coupled nonadiabatic and optical transition in single NVG approximation

To capture the global feature of the wavepacket bifurcation dynamics in the presence of the optical and nonadiabatic interactions, we concentrate mainly on an interplay between optical and nonadiabatic couplings. An initial wavepacket is launched at 4.0 bohrs with a momentum of -30 a.u. on the ground potential surface in Fig. 1(a). To find the basic behavior of the path branching and associated nuclear wavepacket dynamics, we first monitor the population in the excited state of Fig. 1(a) at a time when the branching path remaining on the ground state potential hits its turning point for the first time, which is about 600 a.u. (see Fig. 3) depending on the timing of application of laser. Therefore by this time a single wavepacket experiences only a single optical interaction and a single nonadiabatic interaction. To survey the various situations, we scan the timing of application of laser (t_c) and its field strength (E_s) for two selected laser frequencies (ω).

We first examine the present theory with use of only a single path (or a single Gaussian function) that is prepared to mimic the dynamics of quantum wavepacket for a given initial condition. Further, in the practical application of PSANB scheme, each path is made bifurcated only once by each interaction. Therefore a single path will branch into four pieces after it passes through the nonadiabatic and optical interaction regions if they are well separated. However, if these regions overlap significantly, they are regarded as a single interaction having double maxima or even a single peak (see Fig. 2, upper panel), giving birth to only two branching paths after all.

The practice of path branching in the present work is as follows. We predetermine a threshold value A to judge that the path enters a coupling region (Fig. 2). The phase-space averaging to generate a non-Born–Oppenheimer path with use of the matrix force is performed in this region. Then, the

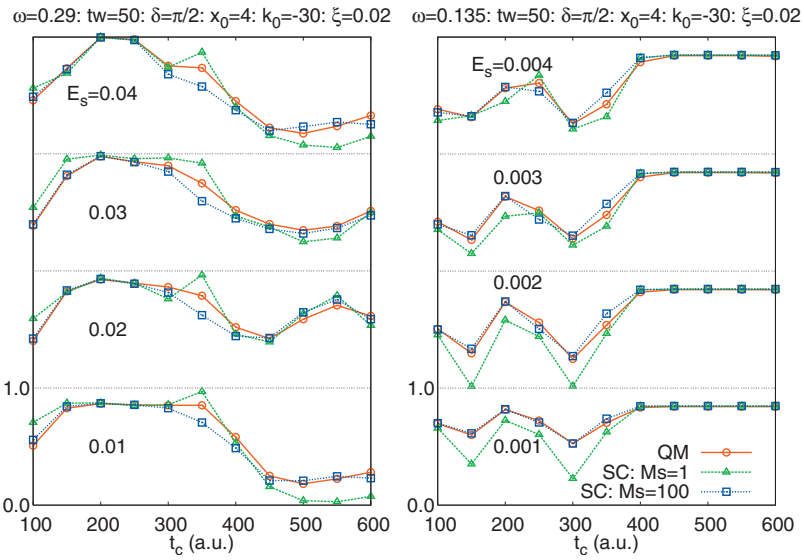

FIG. 4. Population in the excited state at a time when the ground state counterpart hits its first turning point. It is plotted against the timing of shining laser (pulse peak time t_c). The strength of the laser (E_s) is varied from one panel to another as indicated in each box. The left column is with the laser frequency $\omega=0.29$, while the right $\omega=0.135$. In each panel, the results of three methods are presented: (red) full quantum, (green) PSANB-ADF-NVG of a single NVG, and (blue) PSANB-ADF-NVG using a hundred NVGs.

maximum height of $\|V\|$, say, B is automatically detected, which depends on the laser energy, the velocity of nuclei, and so on. At a point where the height of $\|V\|$ becomes as low as $B\times\xi_1$, where the ratio ξ_1 is also a predetermined parameter, we let the path branch into two pieces. When the optical and nonadiabatic interactions significantly overlap with each other, the value of $\|V\|$ may not become smaller than $B\times\xi$ until the two interactions are over entirely. In this case, the two overlapping interactions are regarded as a single interaction.

Figure 4 shows such transition probabilities as a function of the laser timing t_c [see Eq. (61) for a single pulse, $t_c=t_{c1}$]. Each panel adopts different laser intensities E_s. In the left column panels, we set $\omega=0.29$ for the laser frequency, while $\omega=0.135$ in the right column. The other parameters are summarized on top of the figure. The red and solid curves (connected by circles) show the probability given by the full quantum calculations. The green dotted curves (connected by triangles) represent the values of the simplest PSANB-ADF-NVG scheme. (The blue dotted curves connected with squares will be described later.) In almost all the cases examined, such a simple treatment has quantitatively reproduced the global feature of the quantum mechanical transition probability. This is already in a satisfactory level.

The frequency of $\omega=0.29$ (left column of Fig. 4) corresponds to the energy gap at $R=\pm3.2$ bohrs. As observed, the transition probability after $t_c=300$ becomes smaller than before. As seen in Fig. 3, the wavepacket is just passing through the nonadiabatic region around $t=215$. The graphs suggest that the population promoted to the excited state by the nonadiabatic interaction, which is about 84% of the initial population, is much deactivated to the ground state by stimulated emission. It is also worthwhile to note that such an deactivation in $t_c>300$ strongly depends on the field strength applied (compare the panels in left column in $t_c>300$), which is a consequence of Rabi oscillation.[50]

We next study the case of $\omega=0.135$, the right column of Fig. 4. This frequency can tune a resonance excitation between the energy levels at $R=\pm1.5$. The field strength scanned for this frequency has been chosen small enough such that the Rabi oscillation does not affect the dynamics. In these panels, we immediately notice a large transition probability in the domain of $t_c>400$, the magnitude of which is as large as the nonadiabatic transition probability (0.84). Therefore this late shining of the laser of these intensities does not cause an efficient optical transition. On the other hand, we observe two large dips, which are located at $t_c=150$ and 300. It is in these timings that the wavepackets are running in the regions of resonant transition. As for the case of $t_c=150$, the wavepacket on the ground state is pretty much depleted by the resonant optical excitation to the excited state. The remaining packet then undergoes nonadiabatic transition, being pumped up to the excited state. Thus the probability to find in the excited state is reduced. On the other hand, in the case of $t_c=300$, much of the initial wavepacket (actually about 80%) is already transferred to the excited state by the nonadiabatic interaction. The packets thus running on the excited state are pulled down by the optical interaction around $t=300$, which also reduces the relevant probability. Again, the strength is so weak that the Rabi oscillation does not affect such a mechanism to produce two dips in the graphs.

To further comprehend what actually happens to the wavepackets in space-time, we track the dynamics in one of the case studies to a little longer time range. See Fig. 5. A packet comes in from the right hand side and bifurcates into two pieces due to nonadiabatic interaction. Then after some time, they are reorganized by the optical mixing. The excited state wavepacket returns to the avoided crossing region and bifurcated into two pieces, well before the ground state packet reaches this area. The tracks of the paths in bond length along with their quantum counterparts are plotted in panels (a) and (b), and the time-dependent population in the excited states is compared with the quantum mechanical values in panel (c). The electric field transformed from the vector potential is drawn in panel (d). Panel (e) shows the selected snapshots of the history up to $t=950$, which strongly suggests that the phases arising from both electronic and nuclear parts are correctly treated. The phase-space portrait of the path in panel (f) indicates that it has undergone

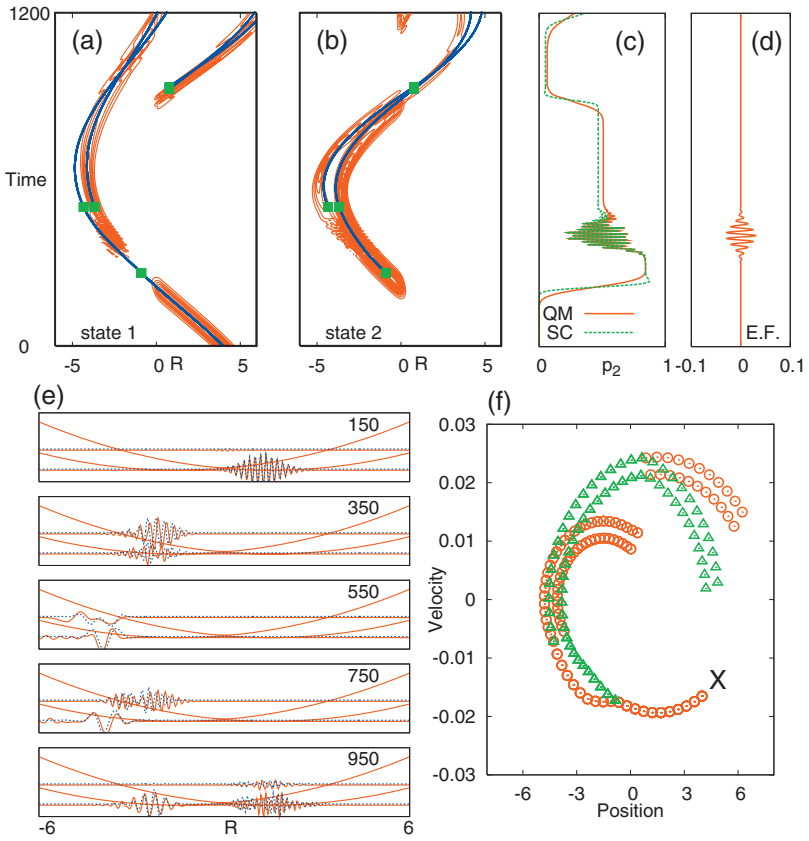

FIG. 5. Wavepacket bifurcation by the optical and nonadiabatic interactions in the order of nonadiabatic → optical → nonadiabatic. The field strength is $E=0.03$. The pulse peak time t_c, time width t_w, central frequency ω, and envelope phase δ are 400, 50, 0.29, and $\pi/2$, respectively. Branching parameters is $\xi_1=0.02$. (a) Track of the branching paths (blue curves) and the quantum wavepacket (red distribution) on the ground state in the R coordinate. Branching takes at points marked with green squares. (b) Those in the excited state. (c) Population in the excited state as a function of time in full quantum (red) and PSANB (green) calculations. (d) Timing of the optical interaction applied. (e) The real part of the nuclear wavepackets of PSANB-ADF-NVG (blue) and full quantum (red). (f) Phase-space portrait of a path of three-time branchings. See the text for details.

branching three times. It starts at a point marked with X. The paths running on the lower potential energy curve are represented in red circles (a discrete time representation of continuous dynamics), and those on the upper one are marked with green triangles. These plots are responsible only for the phase-space geometry of the paths and have no relation to information about quantum phase. At each point of path branching, two children paths emerge continuously both in configuration and momentum spaces. However, the connection to their parent path is not smooth in general in that their derivatives are not continuous at the branching points due to the sudden change in the "forces." However, notice that they do not jump (or hop) discontinuously in either configuration or momentum space.

As seen in the figures, our wavepacket approach shows a good agreement with the quantum mechanical counterpart. The noteworthy features of the wavepacket dynamics observed yet not shown in the figure are summarized as follows. (i) Nonadiabatic transition approximately conserves the central mechanical energy of the nuclear wavepacket, which is compatible with the Condon principle. (ii) Optical dumping near the turning point creates a component of the packet with low wave number. A robust realization of such a splitting may be useful in the study of control of quantum entanglement in quantum information.

C. Multiple NVG representation

Although the simplest approximation to the PSANB-ADF-NVG works well for its compactness, we nonetheless would like to attempt to reduce the error observed in Fig. 4. A straightforward idea to do so is to increase the number of the initial Gaussian functions. Panel (c) of Fig. 5 clearly illustrates one of the limitations of the single Gaussian representation in which the transition probabilities as a function of time for quantum mechanics and the single Gaussian approximation are compared. It is readily noticed that the starting time of nonadiabatic transition in a full quantum calculation always precedes that of the single Gaussian. This is simply because the Gaussian begins to undergo transition only when its center enters the strong coupling region, while the full quantum packet does as soon as only the edge of it enters. We refer to this phenomenon as late-kick-off problem, which was studied earlier by Martínez *et al.*[26] The reverse phenomenon can be seen when the semiclassical path point exits the interaction region. We therefore examine the use of multiple NVGs centered at different phase-space points to mimic a single quantum wavepacket.

To sample the initial points in classical phase space, we utilize the Wigner phase-space distribution function as a weighting function in Monte Carlo importance sampling. Choosing a full quantum wavepacket at $t=0$ as

$$\psi_0(x) = \left(\frac{1}{2\pi\delta^2}\right)^{1/4} \exp\left(-\left(\frac{x-x_0}{2\delta}\right)^2\right) \exp(ik_0(x-x_0)), \tag{67}$$

we have the Wigner function

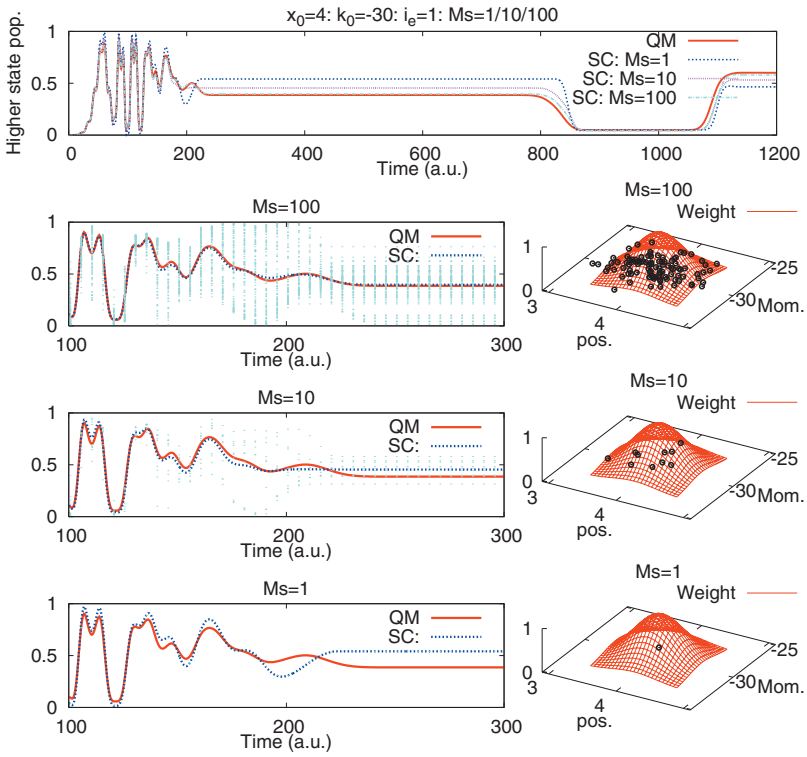

FIG. 6. Convergence of PSANB-ADF-NVG expansion checked with the excited state population dynamics by increasing the number of sampling points (Ms) for the initially prepared Gaussians. Top panel presents the population dynamics throughout the entire dynamics, (solid red) full quantum, (dotted blue) PSANB-ADF-NVG with Ms=1, (dotted red) Ms=10, and (chained blue) Ms=100. The second row compares the full quantum and Ms=100 calculations. The right hand panel schematically shows an importance sampling of the initial condition from phase space. Likewise, the third and fourth rows compare the full quantum results with those of Ms=10 and Ms=1, respectively.

$$W(x,k;x_0,k_0) \equiv \int_{-\infty}^{\infty} \psi_0^*\left(x+\frac{z}{2}\right)\psi_0\left(x-\frac{z}{2}\right)\exp(ikz)dz$$
$$= \exp\left(-2\left(\frac{x-x_0}{2\delta}\right)^2 - 2\delta^2(k-k_0)^2\right), \quad (68)$$

where we modulated a prefactor so as to make the value of function unity at sampling center (x_0,k_0). An initial Gaussian width is determined as $\delta=10/k_0$. We set a sampling region as

$$x \in [x_0-4\delta, x_0+4\delta], \quad k \in \left[k_0-\frac{2}{\delta}, k_0+\frac{2}{\delta}\right], \quad (69)$$

where the wave number k and classical momentum p are related via $p=\hbar k$. With the importance sampling technique, as schematically exemplified in Fig. 6, we let paths start running. The excited state population is simply calculated in a decoherent manner as

$$P_2^{\mathrm{dec}}(t) = \frac{1}{\mathrm{Ms}}\sum_{s}^{\mathrm{Ms}}\sum_{ks}^{\text{excited state}} |C_{2ks}(t)|^2, \quad (70)$$

where $C_{2ks}(t)$ is an excited state electronic amplitude on the path ks and Ms indicates the number of paths initially prepared.

The effect of increasing the sampling points is clearly observed in Fig. 6. In this example, a wavepacket running on the ground potential surface toward the left is first shined by laser and then experiences nonadiabatic transition soon after it. The field parameters, E_s, t_c, t_w, ω, and δ are 0.03, 100, 50, 0.29, and $\pi/2$, respectively. It is very clearly confirmed that as Ms is increased, the results approach the exact quantum values. In the present example, Ms=100 is enough to attain almost the exact values.

Next we look back at Fig. 4. It is noticed that a very good improvement has been achieved in the curve of Ms =100 (represented by blue dotted curve). In most cases there, the multiple NVG representation is seen to improve the single Gaussian approximation raising to almost the exact level. We show later an illustrative example of remedy of the late-lick-off problem.

D. Further refinement to treat overlapping couplings of nonadiabatic and optical interactions

Despite the above improvement, we still observe somewhat a noticeable discrepancy between the full quantum and the calculation of Ms=100 at $t_c=350$ in the left column of Fig. 4. We next explore what is left wrong in the present numerical practice. A close look at the path branching in the case of $t_c=350$ with $E_s=0.03$ shows that the nonadiabatic and optical interactions overlap in such a manner that our simple practice of branching of the paths does not work well. The path first feels the nonadiabatic interaction, and before it finishes the optical interaction begins (see the bottom row of Fig. 7). As seen in the profile of the two successive interactions, a valley of nonzero height is formed in between the two peaks of $\|V\|$. In the present case, the height is low but happens to be a little higher than the threshold value $B\times\xi_1$ that defines to specify the exit of the interaction region. Therefore no branching took place in this valley, and only two paths are generated after all.

To remedy this situation, we allow the path to branch in the valley area after the first (optical) interaction is almost over by setting a new threshold, which is actually higher than the value $B\times\xi_1$. The three panels in the left column of Fig. 7 display the results of no branching in the valley. The middle column panels show the results obtained by setting a

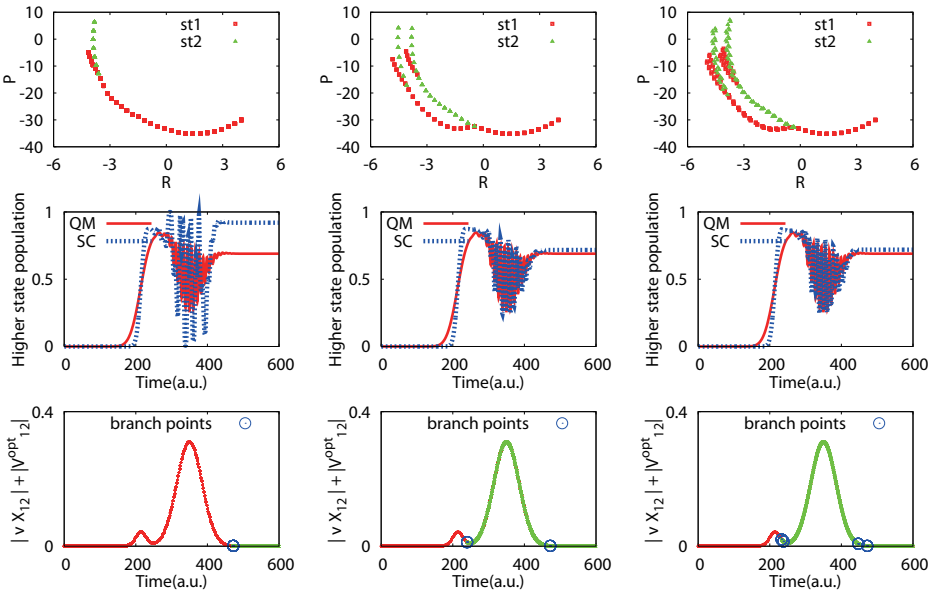

FIG. 7. Effect of cascade branchings on the electronic population dynamics. (left column) One branching at the exit with $\xi_1=0.02$. (Middle) Two time branchings: one in the valley with $\xi_2=0.3$ and another at the exit with $\xi_1=0.02$. (Right) Four time branchings: twice in the valley with $\xi_4=0.5$, $\xi_3=0.34$ and two times at the exit with $\xi_2=0.18$ and $\xi_1=0.02$. The field strength is $E_s=0.03$. The pulse peak time t_c, time width t_w, central frequency ω, and envelope phase δ are 350, 50, 0.290, and $\pi/2$, respectively. The first row panels represent phase-space profile of path branching. The second row panels compare the population dynamics in the excited state given by PSANB-ADF-NVG (Ms=1, blue) and full quantum mechanics (red). The bottom panels mark the positions of path branching.

higher threshold for branching, say, $B\times\xi_2$ (the phase-space profile of branching is shown in the first row). Note that this threshold value is also applied to the final exit. We observe therefore four paths after all. A dramatic improvement is observed in the population of the excited state (see the second row in Fig. 7).

Further improvement can be attained by allowing for more branchings. We let the path branch two times in the valley area with the threshold parameters ξ_4 and ξ_3 and further let it branch two more times at the exit with the parameters ξ_2 and ξ_1 (see the caption of Fig. 7 for the detail). This makes the path branch into 16 (2^4) pieces in total after all the interactions are over. Thus, the better transition probability has been obtained, but the price is that the computational tasks increase.

Finally, we should recall that the deviation of thus improved PSANB from the full quantum value found around $t=200$ in Fig. 7 (see the panel at rightmost column and second row) is due to the single NVG representation, the so-called late-kick-off by the single Gaussian. Just to support this argument numerically, we exhibit Fig. 8 to illustrate that the multiple sampling of the wave function can indeed remedy this shortcoming. The time-dependent population to be found at the upper potential curve is computed with Ms=1, 10, 100, and 1000 in comparison with the exact quantum values. As seen in the graphs, the Ms=10 has improved the late-kick-off behavior to a sufficient extent, and the present results further approach the exact values as Ms is raised to 100 and 1000 monotonically without numerical instability.

E. HF molecule: An illustrative example toward real systems

The second system we choose is HF molecule. The primary aim of this case-study is to show that the present method is actually being applied to real systems on *ab initio* basis. Only the lowest two Σ adiabatic states are considered. The potential energy function together with the spatial distributions of nonadiabatic coupling element and TVM are plotted in Fig. 1(b). The TVM has a peak around the ground state minimum, and its magnitude gradually decreases with an increase in the bond distance.

To produce these data, we carried out a three-state averaged full-valence complete active space self-consistent-field calculation with 6-31G basis set by using MOLPRO package.[51] To facilitate the computation, we fitted the potential functions in the functional form of multipolynomial of square root Morse functions $V(R)=\Sigma_{n=0}^{N}a_n(1-\exp(-b(R-R_0)))^n$, while the coupling matrix elements were fitted to linear combinations of Gaussian functions by optimizing the linear coefficients and the Gaussian exponents, while the central positions were determined beforehand. The full quantum calculations have been performed for this system, too. The derivative operator and position operator were treated in sinc discrete variable representation[49] with 600 grid points uniformly distributed from $R=0$ to 16 bohrs. The initial position and momentum are set to 6.0 bohrs and -30 a.u., respectively.

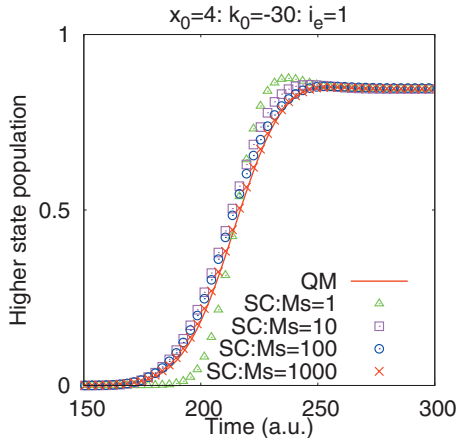

FIG. 8. Remedy of the late-kick-off problem arising from a single path approximation in terms of the multiple sampling. Red solid curve represents the full quantum probability to find the population in the excited state by the nonadiabatic coupling. Green triangles give the similar probability computed with a single initial sampling condition (Ms=1) exhibiting the feature of late-kick-off, while pink square, blue circle, and red cross represent the results of Ms=10, 100, and 1000, respectively.

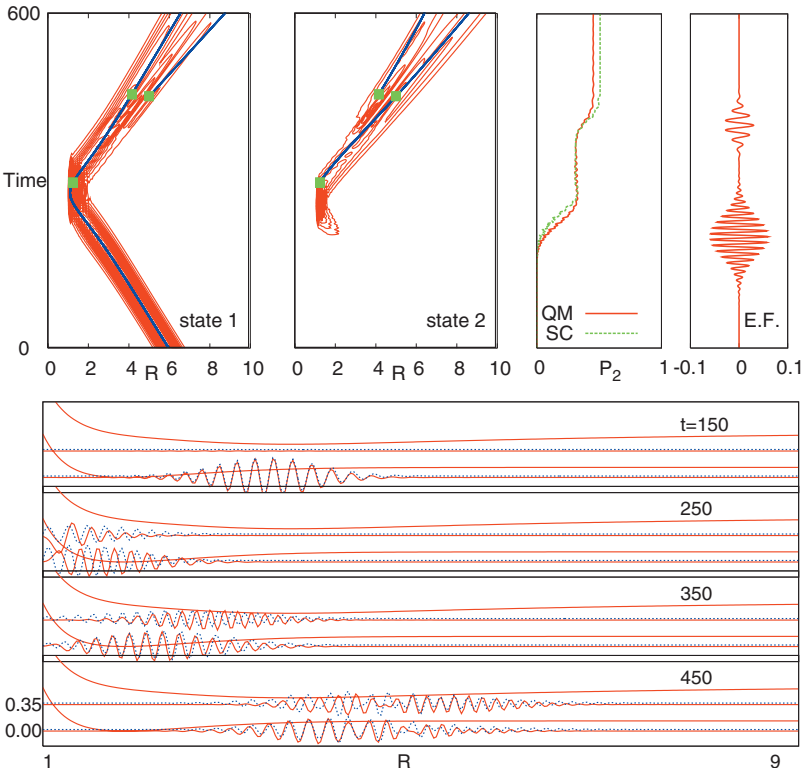

FIG. 9. Two pulse shining on HF molecule causing two time branchings. The field strengths are $E_{s_1}/E_{s_2}=0.06/0.03$. The pulse peak time $t_{c1/2}$, time width $t_{w1/2}$, central frequency $\omega_{1/2}$, and envelope phase $\delta_{1/2}$ are 200/400, 50/30, 0.6/0.35, and $(\pi/2)/(\pi/2)$, respectively. The upper four panels exhibit the same kind of quantities as those of panels (a)–(d) in Fig. 5, respectively. In the four lower panels, solid red curve and dotted blue curves represent the real part of the wavepackets given by full quantum and PSANB-ADF-NVG results.

The computational level of PSANB here is the lowest, namely, a path of single sampling for an initial condition. We apply two delayed laser pulses on the molecule. Path branching is performed only after each isolated optical interactions is over, and the phase-space averaging is applied in the nonadiabatic region without branching. The initial conditions are given in the caption of Fig. 9. A single wavepacket is seen to split into four pieces by the two successive isolated pulses: two packets running on the ground state, while the other two running on the excited state.

The field frequency and peak time of the first pulse were determined so that the branching should occur near the classical turning point. While the frequency of the second pulse was determined such that the packets running in the dissociation channel on the ground state surface can make a resonant transition somewhere in a region indicated in Fig. 9 (the place of the second bifurcation). Taking into account the large momentum of the bouncing wavepacket, the second pulse duration was set to a slightly shorter value than the first one. The strengths of these pulses were determined to be $E_{s_2}=0.06$ and $E_{s_2}=0.03$ in a rather arbitrary fashion.

Again it is well confirmed from those figures that the present wavepacket scheme reproduces the full quantum results to a very good extent for this simple treatment, although the PSANB-ADF-NVG slightly overestimates the transition population. The splitting of wave functions at $t=450$ a.u. is qualitatively well described with respect to its broadening and wave numbers. This simplest numerical result strongly suggests that the present theory is promising to treat realistic molecular systems placed in a complicated laser field.

V. CONCLUDING REMARKS

In this paper we have established a useful quantum chemical theory to describe nonadiabatic dynamics in laser fields, where our formerly proposed non-Born–Oppenheimer path concept plays an important role. These paths can branch continuously due to nonadiabatic coupling, optical interactions, and their coexistence. These nonclassical paths are quantized with our proposed semiclassical mechanics in terms of NVGs. Though we limited our sample calculations to one-dimensional systems, its multidimensional extension is rather straightforward and will be reported in the near future. The electronic wavepacket bifurcation is realized along these non-Born–Oppenheimer paths simultaneously. The total electronic and nuclear wave functions thus produced in *ab initio* manner correctly carry the phase information arising from the optical and nonadiabatic interactions.

The main concern in this paper has been to establish and verify the methodological aspect of the theory. In doing so, we have mainly utilized the nuclear wavepackets in comparison with the full quantum counterparts. However, the major advantage of the present theory is that the electronic wavepackets are faithfully generated according to the coupling interactions applied in attosecond dynamics induced by ultrashort and/or intense pulse lasers. Applications of the present theory focusing more on the physical aspects will be reported in our future publications.

ACKNOWLEDGMENTS

The authors thank Dr. Y. Arasaki, Dr. S. Takahashi, and Dr. M. Kanno for valuable discussions. This work has been supported by Grant-in-Aid for Scientific Research from Japan Society for the Promotion of Science.

APPENDIX A: QUANTUM MOLECULAR DYNAMICS WITH MULTISTATES

An outline for our practice in full quantum mechanical calculations of nonadiabatic dynamics in laser fields is described here, with which we prepare reference data to assess the quality of PSANB-ADF-NVG method in vector potentials.

1. Coupled nuclear dynamics under laser field

We present coupled dynamics in a full Cartesian space exemplifying only two-level system for simplicity. Extension to more general cases is rather straightforward. The multistate coupled equations of motion for nuclear wavepacket in Eq. (1) are expressed by

$$i\hbar\dot{\chi}_\alpha = \sum_N \hat{T}_N\chi_\alpha - i\hbar\sum_N\sum_\beta \mathbf{X}^N_{\alpha\beta}\hat{\mathcal{V}}_N\chi_\beta - \frac{\hbar^2}{2}\sum_N\sum_\beta \frac{Y^N_{\alpha\beta}}{M_N}\chi_\beta + \sum_\beta \mathcal{H}^{(\mathrm{el})}_{\alpha\beta}\chi_\beta, \tag{A1}$$

where again $\mathcal{H}^{(\mathrm{el})}$ is an electronic Hamiltonian including external vector potential term. In this expression, $\hat{T}_N \equiv (1/2M_N)(\hat{\mathbf{P}}_N - (Z_N e/c)\mathbf{A}_N)^2$ and $\hat{\mathcal{V}}_N \equiv (1/M_N)(\hat{\mathbf{P}}_N - (Z_N e/c)\mathbf{A}_N)$ are the kinematic energy and velocity operator for the Nth nucleus in a vector field, respectively, and $\hat{\mathbf{P}} = -i\hbar\nabla_N$ is a (canonical) momentum. Interactions between particle spin and vector field are neglected since they are generally very weak.[52,53] M_N and $Z_N e$ are mass and charge of the nucleus N, respectively. The suffixes α and β specify adiabatic states. The vector field potential at a nuclear position $\mathbf{R}_N=(x_N,y_N,z_N)$ is expressed by $\mathbf{A}_N=\mathbf{A}_N(\mathbf{R}_N)$. $\mathbf{X}^N_{\alpha\beta} \equiv \langle\alpha|\nabla_N|\beta\rangle$ and $Y^N_{\alpha\beta} \equiv \langle\alpha|\Delta_N|\beta\rangle$ are the first and second order nuclear derivative coupling matrix elements, respectively. The electronic Hamiltonian matrix including vector potential term is expressed as $\mathcal{H}^{(\mathrm{el})}_{\alpha\beta} = \epsilon_\alpha\delta_{\alpha\beta} + V^{(\mathrm{opt})}_{\alpha\beta}$, where ϵ_α is a field-free adiabatic energy of αth electronic state and $V^{(\mathrm{opt})}_{\alpha\beta}$ denotes a matrix representation of an operator

$$\hat{V}^{(\mathrm{opt})} = \frac{1}{2m_e}\sum_j^{\mathrm{el}}\left(\hat{\mathbf{p}}_j + \frac{e}{c}\mathbf{A}_j\right)^2 - \frac{1}{2m_e}\sum_j^{\mathrm{el}}\hat{\mathbf{p}}_j^2. \tag{A2}$$

By applying the long wave approximation for an external vector potential and carrying out the appropriate Hermitization with respect to the nuclear derivative couplings,[35] Eq. (A1) is transformed into the working equations of motion (in the velocity form representation),

$$i\hbar\begin{pmatrix}\dot{\chi}_1\\ \dot{\chi}_2\end{pmatrix} = \begin{pmatrix}\hat{H}_{11} & \hat{H}_{12}\\ \hat{H}_{21} & \hat{H}_{22}\end{pmatrix}\begin{pmatrix}\chi_1\\ \chi_2\end{pmatrix}, \tag{A3}$$

where diagonal ($\alpha=\beta$) and off-diagonal ($\alpha\neq\beta$) parts are given by

$$\hat{H}_{\alpha\alpha} = \sum_N \frac{-\hbar^2}{2M_N}\Delta_N - \frac{e\hbar}{ic}\mathbf{A}\sum_N\frac{Z_N}{M_N}\nabla_N + \epsilon_\alpha - \frac{\hbar^2}{2}\sum_N\frac{Y^N_{\alpha\alpha}}{M_N} \tag{A4}$$

and

$$\hat{H}_{\alpha\beta} = -\frac{\hbar^2}{2}\sum_N\frac{\tilde{\nabla}_N\mathbf{X}^N_{\beta\alpha} + \mathbf{X}^N_{\alpha\beta}\vec{\nabla}_N}{M_N} + i\hbar\frac{e}{c}\mathbf{A}\sum_N\frac{Z_N}{M_N}\mathbf{X}^N_{\alpha\beta} + W_{\alpha\beta}, \tag{A5}$$

respectively, where the dominant optical transition is caused by the term $W_{\alpha\beta}=W^*_{\beta\alpha}=\frac{e\hbar}{icm_e}\mathbf{A}\langle\alpha|\Sigma^{\mathrm{el}}_j\nabla_j|\beta\rangle$ in the off-diagonal part. The nonlocal operator term $-(e\hbar/ic)\mathbf{A}\Sigma_N(Z_N/M_N)\nabla_N$ serves as a time-dependent, external nonlocal potential operator acting on the nuclear wavepacket, affecting their tracks and shapes.

2. Reduction to one-dimensional case of diatomic molecule

One-dimensional simplification is made as follows.

a. Nuclear derivative coupling

Consider two particles 1 and 2 at x_1 and x_2 on x axis. Supposed $x_1<x_2$, an atom distance is given by $r\equiv x_2-x_1$. Then, their differential relation becomes $\Delta r(\Delta x_2,\Delta x_1)=\Delta x_2-\Delta x_1$, which contains a redundancy. Therefore, we impose the condition for conservation of total momentum, $M_1\Delta x_1+M_2\Delta x_2=0$. Then we obtain $\Delta r=-[(M_1+M_2)/M_2]\Delta x_1=[(M_2+M_1)/M_1]\Delta x_2$. Through a careful derivation using this condition and definition of derivative, the proposed derivative coupling is written down as

$$\langle\alpha|\frac{\partial}{\partial r}|\beta\rangle = -\frac{M_2}{M_1+M_2}\langle\alpha|\frac{\partial}{\partial x_1}|\beta\rangle + \frac{M_1}{M_1+M_2}\langle\alpha|\frac{\partial}{\partial x_2}|\beta\rangle. \tag{A6}$$

b. Quantum counterparts of electric force on nuclei and field-derivative coupling

We consider the second terms in Eqs. (A4) and (A5). The field induced acceleration for r is written as $(Z_2e/M_2-Z_1e/M_1)E$, where $E(t)$ is a time-dependent electric field. The corresponding electric force becomes $\mu(Z_2e/M_2-Z_1e/M_1)E(t)$, which constitutes an effective charge, $q^{\mathrm{eff}}\equiv\mu(Z_2/M_2-Z_1/M_1)e$, with $\mu=M_1M_2/(M_1+M_2)$ being the reduced mass. These observations yield a concerned one-dimensional modeling expressed as

$$-\frac{e\hbar}{ic}\mathbf{A}\sum_N\frac{Z_N}{M_N}\nabla_N \Rightarrow -\frac{e\hbar}{ic}A\left(\frac{Z_2}{M_2}-\frac{Z_1}{M_1}\right)\partial_r \tag{A7}$$

and

$$+i\hbar\frac{e}{c}\mathbf{A}\sum_N\frac{Z_N}{M_N}\mathbf{X}^N_{12} \Rightarrow +i\hbar\frac{e}{c}A\left(\frac{Z_2}{M_2}-\frac{Z_1}{M_1}\right)X_{12}. \tag{A8}$$

c. One-dimensional model for diatomic molecule

Using the expressions stated above, a coupled equations of motion is written down in a compact form,

$$i\hbar\begin{pmatrix}\dot{\chi}_1\\ \dot{\chi}_2\end{pmatrix}=\begin{pmatrix}-\frac{\hbar^2}{2\mu}\frac{\partial^2}{\partial r}+\hat{\eta}+\epsilon_1 & \hat{\gamma}_{12}+\hat{\xi}_{12}+W_{12}\\ \hat{\gamma}_{21}+\hat{\xi}_{21}+W_{21} & -\frac{\hbar^2}{2\mu}\frac{\partial^2}{\partial r}+\hat{\eta}+\epsilon_2\end{pmatrix}\begin{pmatrix}\chi_1\\ \chi_2\end{pmatrix}, \tag{A9}$$

where $\hat{\eta}\equiv-(e\hbar/ic)A(Z_2/M_2-Z_1/M_1)\partial_r$ serves as an external nonlocal potential operator on the wavepacket assigned to a single state surface, $\hat{\gamma}_{\alpha\beta}\equiv-(\hbar^2/2)(\bar{\partial}_r X_{\beta\alpha}+X_{\alpha\beta}\vec{\partial}_r)/\mu$ causes a nonadiabatic transition between different states, and $\hat{\xi}_{\alpha\beta}\equiv+i\hbar(e/c)A(Z_2/M_2-Z_1/M_1)X_{\alpha\beta}$ takes a form of direct coupling between an external optical field and the molecular inherent nonadiabaticity. Here again, $W_{\alpha\beta}$ is the dominant source of optically induced electric transition.

[1] A. Stolow, A. E. Bragg, and D. N. Neumark, Chem. Rev. (Washington, D.C.) **104**, 1719 (2004).
[2] S. H. Lin, A. A. Villaeys, and Y. Fujimura, *Advances in Multi-Photon Processes and Spectroscopy* (World Scientific, Singapore, 2004).
[3] P. Farmanara, H. H. Ritze, V. Stert, W. Radloff, and I. V. Hertel, J. Chem. Phys. **111**, 633 (1999); **115**, 277 (2001); **116**, 1443 (2002).
[4] I. V. Hertel and W. Radloff, Rep. Prog. Phys. **69**, 1897 (2006).
[5] M. Seel and W. Domcke, J. Chem. Phys. **95**, 7806 (1991).
[6] Y. Arasaki, K. Takatsuka, K. Wang, and V. McKoy, Phys. Rev. Lett. **90**, 248303 (2003); J. Chem. Phys. **90**, 248303 (2003); **119**, 7913 (2003).
[7] K. Takatsuka and T. Yonehara, Adv. Chem. Phys. **144**, 93 (2009).
[8] M. S. Child, *Molecular Collision Theory* (Academic, London, 1974); M. S. Child, *Semiclassical Mechanics with Molecular Approximations* (Clarendon, Oxford, 1991).
[9] H. Nakamura, *Nonadiabatic Transition* (World Scientific, New Jersey, 2002).
[10] A. Jasper, B. K. Kendrick, C. A. Mead, and D. G. Truhlar, in *Modern Trends in Chemical Reaction Dynamics Part I*, edited by X. Yang and K. Liu (World Scientific, Singapore, 2004), Chap. 8.
[11] W. Domcke, D. R. Yarkony, and H. Köppel, *Conical Intersections: Electronic Structure, Dynamics and Spectroscopy* (World Scientific, New Jersey, 2004).
[12] G. Stock and M. Thoss, Adv. Chem. Phys. **131**, 243 (2005).
[13] M. Baer, *Beyond Born–Oppenheimer* (Wiley, Hoboken, 2006).
[14] L. D. Landau, Phys. Z. Sowjetunion **2**, 46 (1932).
[15] C. Zener, Proc. R. Soc. London, Ser. A **137**, 696 (1932).
[16] E. C. G. Stueckelberg, Helv. Phys. Acta **5**, 369 (1932).
[17] C. Zhu and H. Nakamura, J. Chem. Phys. **102**, 7448 (1995).
[18] C. Zhu and H. Nakamura, J. Chem. Phys. **106**, 2599 (1997).
[19] J. C. Tully and R. Preston, J. Chem. Phys. **55**, 562 (1971).
[20] J. C. Tully, J. Chem. Phys. **93**, 1061 (1990).
[21] T. J. Martínez, M. Ben-Nun, and R. D. Levine, J. Phys. Chem. **100**, 7884 (1996).
[22] T. J. Martínez, M. Ben-Nun, and R. D. Levine, J. Phys. Chem. **101**, 6389 (1997).
[23] M. D. Hack, A. M. Wensman, D. Truhlar, M. Ben-Nun, and T. J. Martínez, J. Chem. Phys. **115**, 1172 (2001).
[24] T. J. Martínez, Acc. Chem. Res. **39**, 119 (2006).
[25] A. M. Virshup, C. Punwong, T. V. Pogorelov, B. A. Lindquist, C. Ko, and T. J. Martínez, J. Phys. Chem. B **113**, 3280 (2009).
[26] S. Yang, J. D. Coe, B. Kaduk, and T. Martínez, J. Chem. Phys. **130**, 134113 (2009).
[27] H.-D. Meyer and W. H. Miller, J. Chem. Phys. **70**, 3214 (1979).
[28] M. Amano and K. Takatsuka, J. Chem. Phys. **122**, 084113 (2005).
[29] A. W. Jasper, M. D. Hack, A. Chakradorty, D. G. Truhlar, and P. Piecuch, J. Chem. Phys. **115**, 7945 (2001).
[30] C. Zhu, S. Nangia, A. W. Jasper, and D. G. Truhlar, J. Chem. Phys. **121**, 7658 (2004).
[31] C. Zhu, A. W. Jasper, and D. G. Truhlar, J. Chem. Phys. **120**, 5543 (2004).
[32] X. Sun and W. H. Miller, J. Chem. Phys. **106**, 6346 (1997).
[33] N. Ananth, C. Venkataraman, and W. H. Miller, J. Chem. Phys. **127**, 084114 (2007).
[34] K. Takatsuka, J. Phys. Chem. A **111**, 10196 (2007).
[35] T. Yonehara and K. Takatsuka, J. Chem. Phys. **129**, 134109 (2008).
[36] K. Takatsuka and A. Inoue, Phys. Rev. Lett. **78**, 1404 (1997); A. Inoue-Ushiyama and K. Takatsuka, Phys. Rev. A **59**, 3256 (1999).
[37] K. Takatsuka, Int. J. Quantum Chem. **109**, 2131 (2009).
[38] T. Yonehara, S. Takahashi, and K. Takatsuka, J. Chem. Phys. **130**, 214113 (2009).
[39] T. Yonehara and K. Takatsuka, Chem. Phys. **366**, 115 (2009).
[40] M. Born and K. Huang, *Dynamical Theory of Crystal Lattices* (Oxford University Press, Oxford, 1954).
[41] K. Takatsuka, J. Chem. Phys. **124**, 064111 (2006).
[42] T. Yonehara and K. Takatsuka, J. Chem. Phys. **128**, 154104 (2008).
[43] Y. Aharonov and D. Bohm, Phys. Rev. **115**, 485 (1959).
[44] G. Herzberg and H. C. Longuet-Higgins, Discuss. Faraday Soc. **35**, 77 (1963).
[45] M. V. Berry, Proc. R. Soc. London **A392**, 45 (1984).
[46] S. Takahashi and K. Takatsuka (unpublished).
[47] H. Yoshida, Phys. Lett. A **150**, 262 (1990).
[48] H. Tal-Ezer and R. Kosloff, J. Chem. Phys. **81**, 3967 (1984).
[49] D. T. Colbert and W. H. Miller, J. Chem. Phys. **96**, 1982 (1992).
[50] I. I. Rabi, Phys. Rev. **51**, 652 (1937).
[51] H.-J. Werner, P. J. Knowles, R. D. Amos *et al.*, MOLPRO, version 2006.1, a package of *ab initio* programs.
[52] I. Last and M. Baer, J. Chem. Phys. **82**, 4954 (1985).
[53] Y. I. Salamin, S. X. Hu, Z. Hatsagortsyan, and C. H. Keitel, Phys. Rep. **427**, 41 (2006).